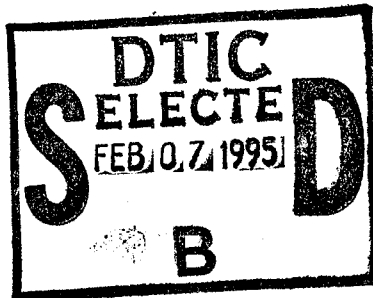


# **NAVAL POSTGRADUATE SCHOOL MONTEREY, CALIFORNIA**



## **THESIS**

**RADAR CROSS SECTION SYNTHESIS FOR  
PLANAR RESISTIVE SURFACES**

by

Nikolaos I. Faros

December, 1994

Thesis Advisor:

David C. Jenn

**Approved for public release; distribution is unlimited.**

DTIC QUALITY INSPECTED 3

19950130 037

## REPORT DOCUMENTATION PAGE

Form Approved OMB No. 0704-0188

Public reporting burden for this collection of information is estimated to average 1 hour per response, including the time for reviewing instruction, searching existing data sources, gathering and maintaining the data needed, and completing and reviewing the collection of information. Send comments regarding this burden estimate or any other aspect of this collection of information, including suggestions for reducing this burden, to Washington Headquarters Services, Directorate for Information Operations and Reports, 1215 Jefferson Davis Highway, Suite 1204, Arlington, VA 22202-4302, and to the Office of Management and Budget, Paperwork Reduction Project (0704-0188) Washington DC 20503.

1. AGENCY USE ONLY ( <i>Leave blank</i> )	2. REPORT DATE	3. REPORT TYPE AND DATES COVERED Master's Thesis	
4. TITLE AND SUBTITLE RADAR CROSS SECTION SYNTHESIS FOR PLANAR RESISTIVE SURFACES		5. FUNDING NUMBERS	
6. AUTHOR(S) Faros, Nikolaos I.			
7. PERFORMING ORGANIZATION NAME(S) AND ADDRESS(ES) Naval Postgraduate School Monterey CA 93943-5000		8. PERFORMING ORGANIZATION REPORT NUMBER	
9. SPONSORING/MONITORING AGENCY NAME(S) AND ADDRESS(ES)		10. SPONSORING/MONITORING AGENCY REPORT NUMBER	
11. SUPPLEMENTARY NOTES The views expressed in this thesis are those of the author and do not reflect the official policy or position of the Department of Defense or the U.S. Government.			
12a. DISTRIBUTION/AVAILABILITY STATEMENT Approved for public release; distribution is unlimited.		12b. DISTRIBUTION CODE	
13. ABSTRACT ( <i>maximum 200 words</i> )  Equations are developed for synthesizing the radar cross section (RCS) of a planar resistive sheet. The equations are verified by first calculating the RCS of the sheet for an assumed resistivity function. The computed RCS is used in the synthesis equations, and the resistivity distribution is shown to be in agreement with the original assumed distribution.  Several synthesis parameters are examined and their effect on the accuracy and computing time are discussed. Results are shown for both monostatic and bistatic RCS with arbitrary incident wave polarization.			
14. SUBJECT TERMS RCS, RCS Synthesis, Resistive Sheets		15. NUMBER OF PAGES 116	
		16. PRICE CODE	
17. SECURITY CLASSIFICATION OF REPORT Unclassified	18. SECURITY CLASSIFICATION OF THIS PAGE Unclassified	19. SECURITY CLASSIFICATION OF ABSTRACT Unclassified	20. LIMITATION OF ABSTRACT UL

NSN 7540-01-280-5500

Standard Form 298 (Rev. 2-89)

Prescribed by ANSI Std. Z39-18 298-102



Approved for public release; distribution is unlimited.

**RADAR CROSS SECTION SYNTHESIS FOR PLANAR RESISTIVE  
SURFACES**

by

Nikolaos I. Faros  
Lieutenant J.G., Hellenic Navy  
Hellenic Naval Academy, 1988

Submitted in partial fulfillment  
of the requirements for the degree of

**MASTER OF SCIENCE IN ELECTRICAL ENGINEERING**

from the

**NAVAL POSTGRADUATE SCHOOL**  
**December 1994**

Author: Nikolaos I. Faros

Nikolaos I. Faros

Approved by: David C. Jenn

David C. Jenn, Thesis Advisor

R. Janaswamy

Ramakrishna Janaswamy, Second Reader

Michael A. Morgan

Michael A. Morgan, Chairman

Department of Electrical and Computer Engineering

Accession For	
NTIS GRA&I	<input checked="" type="checkbox"/>
DTIC TAB	<input type="checkbox"/>
Unannounced	<input type="checkbox"/>
Justification	
By _____	
Distribution _____	
Availability Codes	
Dist	Avail and/or Special
P-1	



## **ABSTRACT**

Equations are developed for synthesizing the radar cross section (RCS) of a planar resistive sheet. The equations are verified by first calculating the RCS of the sheet for an assumed resistivity function. The computed RCS is used in the synthesis equations, and the resistivity distribution is shown to be in agreement with the original assumed distribution.

Several synthesis parameters are examined and their effect on the accuracy and computing time are discussed. Results are shown for both monostatic and bistatic RCS with arbitrary incident wave polarization.



## TABLE OF CONTENTS

I.	INTRODUCTION . . . . .	1
II.	THEORETICAL BACKGROUND . . . . .	5
A.	RESISTIVE, CONDUCTIVE AND IMPEDANCE SURFACES . . . . .	5
B.	REFLECTION AND TRANSMISSION . . . . .	7
1.	Parallel Polarization . . . . .	8
2.	Perpendicular (Normal) Polarization . . . . .	11
C.	RADIATION AND SCATTERING EQUATIONS . . . . .	12
III.	FORMULATION AND SOLUTION . . . . .	15
A.	BISTATIC CASE . . . . .	15
1.	Parallel Polarization . . . . .	17
2.	Perpendicular Polarization . . . . .	20
3.	Arbitrary Polarization . . . . .	22
B.	MONOSTATIC CASE . . . . .	23
C.	SYNTHESIS FORM OF THE SCATTERING EQUATIONS . .	25
IV.	COMPUTER IMPLEMENTATION AND DATA ANALYSIS . . . . .	29
A.	GENERAL APPROACH . . . . .	29
B.	BISTATIC CASE . . . . .	31
1.	Parallel Polarization . . . . .	32
2.	Arbitrary Polarization . . . . .	46
C.	MONOSTATIC CASE . . . . .	52
D.	RELATION TO THE SAMPLING THEOREM . . . . .	55
E.	SUMMARY . . . . .	70
V.	CONCLUSIONS . . . . .	71
APPENDIX.	COMPUTER CODES . . . . .	75
LIST OF REFERENCES . . . . .	103	
INITIAL DISTRIBUTION LIST . . . . .	105	



## **ACKNOWLEDGEMENT**

This thesis is dedicated to my parents, Yiannis and Irini, and to my wife Maria, for their help, understanding and support.

## I. INTRODUCTION

The design of radar-stealthy platforms has become an important engineering problem over the last several decades. Although the principles of radar stealth are well known, radar cross section (RCS) prediction and reduction are still difficult tasks. The development of increasingly sophisticated detection systems threatens to reduce the mission effectiveness of many types of weapons platforms. Much effort is now spent on reducing radar detectability by reducing the RCS of the platform.

Four basic techniques are employed in radar cross section reduction (RCSR):

1. shaping,
2. surface material selection,
3. active cancellation, and
4. passive cancellation.

Each method has advantages and disadvantages and the final selection is a compromise. Shaping is one of the most important ways of controlling the radar echo, but usually RCSR at one viewing angle is accompanied by an enhancement at others. Radar absorbing materials (RAM) can also be used, and the RCS reduction for this case is achieved by the dissipation of energy inside of the material. The platform performance (e.g., aerodynamic efficiency) generally decreases due to added weight. Surface maintenance requirements are also more demanding than those for conventional materials. Active and passive cancellation are limited methods and can only be applied to narrow frequency bands and spatial regions.

When choosing materials it is necessary to establish a relationship between the electrical characteristics of the material and the target's scattered field. The electrical

properties of a material are usually expressed in terms of the complex permittivity and permeability ( $\epsilon$  and  $\mu$  respectively). Finding the scattered field when  $\epsilon$ ,  $\mu$  and the shape of the target are known, is straightforward, although not always easy. RCS synthesis, the inverse problem (i.e., finding  $\epsilon$  and  $\mu$  for a given RCS pattern and body shape) is more difficult because, in general, a complicated set of coupled integral equations must be solved. Because of the complexity of the synthesis procedure, RCS reduction using RAM has been based on intuition and experience.

An RCS synthesis method for an impedance surface can be based on the solution of the scattering integral using a method of moments (MM) technique. The (unknown) surface impedance is expanded in a series of basis functions with unknown coefficients. In the most general synthesis case, both electric and magnetic currents must be considered. When the surface is planar, an expression for the currents can be obtained by applying an approximate set of boundary conditions at the surface [Ref. 1]. In general, a coupled set of integral equations must be solved [Ref. 2]. The solution yields the surface impedance at every point on the surface of the body for a specified scattered field (or RCS) pattern. Once the surface impedance is known, the electrical properties of the material can be determined under certain conditions via the refractive index of the material [Ref. 3].

A resistive sheet is a special case of an impedance surface since it does not support magnetic currents. It is of great importance for RCS reduction purposes because it is used to control travelling wave effects. In this thesis, the synthesis procedure described above is applied to a resistive sheet, in which case the integral equations simplify considerably.

Chapter II is a review of the concepts and formulas required in the formulation and solution of the problem. The

reflection and transmission coefficients for a thin resistive surface are also derived from the boundary conditions. In Chapter III the appropriate equations are derived and expressed in matrix form for the monostatic and bistatic cases. Chapter IV deals with the computer implementation of these equations and the evaluation of the obtained data. Finally, Chapter V concludes with a discussion on the benefits, concerns, and recommendations for future work.



## II. THEORETICAL BACKGROUND

In this chapter, a few concepts and equations used throughout the thesis are introduced.

### A. RESISTIVE, CONDUCTIVE AND IMPEDANCE SURFACES

Thin layers of lossy materials are of special interest in RCSR design as they have lower RCS than the corresponding perfect electric conductors [Ref. 3]. A mathematical model of such a layer is an *electrically resistive sheet*. It can be visualized as a thin sheet of highly conducting material whose permeability is that of the surrounding medium (free space). Theoretically, it is composed of an electric surface current of infinitesimal thickness whose total strength is proportional to the tangential electric field at its surface. The sheet is characterized by a jump discontinuity in the tangential components of the magnetic field across the surface, but no discontinuity in the tangential electric field. Therefore, a resistive sheet does not support magnetic currents. Its properties are completely specified by its resistivity,  $R_s$  in ohms per square. This unit is derived from the basic definition of the resistance of a rectangular cell with length  $l$ , and cross section,  $S$ . For the special case of length equal to width ( $l=w$ )

$$R_s = \frac{l}{\sigma S} = \frac{l}{\sigma t w} = \frac{1}{\sigma t} \quad [\Omega] \quad (1)$$

where,  $\sigma$  is the conductivity of the material in (Siemens/meter) and  $t$  is the thickness of the cell.

The boundary conditions at the two sides of the sheet follow from the usual boundary conditions of electromagnetics [Ref. 2]. For the limiting case of  $t$  approaching zero,  $\sigma$  increases in such a manner that  $R_s$  is finite in the limit. However, when  $R_s=0$  the sheet is perfectly conducting, and

when  $R_s = \infty$  it is perfectly transparent. Thus, the boundary conditions for the resistive sheet are [Ref. 4]

$$\Delta H_{\tan} = J_s = \sigma t E_{\tan} = \frac{E_{\tan}}{R_s}$$

$$E_{\tan}(+) = E_{\tan}(-) = R_s J_s$$

where the signs refer to the upper (positive) and lower (negative) faces of the sheet, and  $J_s$  is the total surface electric current supported by the surface.

A general vector form of the boundary conditions are [Ref. 1]

$$\hat{n} \times \vec{E}(+) - \hat{n} \times \vec{E}(-) = 0 \quad (2)$$

$$\hat{n} \times \vec{H}(+) - \hat{n} \times \vec{H}(-) = \vec{J}_s \quad (3)$$

with

$$\hat{n} \times \{\hat{n} \times \vec{E}(\pm)\} = -R_s \vec{J}_s \quad (4)$$

where  $\hat{n}$  is the unit vector normal to the sheet and directed towards the positive (plus) side of the sheet and  $\vec{J}_s$  is the total electric current supported.

The electromagnetic dual of the resistive sheet is the magnetically conductive sheet having a conductivity  $R_m$  in S/sq. Such a sheet has a jump discontinuity in the tangential electric field but none in the magnetic field, and supports only magnetic currents. It simulates a thin layer whose permeability differs from that of the surrounding medium (it would be difficult to realize this type of sheet). When  $R_m = 0$  the sheet acts like a "perfect ferrite" with infinite permeability and when  $R_m = \infty$  it no longer exists. The general boundary conditions for such a sheet are

$$\hat{n} \times \vec{H}(+) - \hat{n} \times \vec{H}(-) = 0$$

$$\hat{n} \times \vec{E}(+) - \hat{n} \times \vec{E}(-) = -\vec{J}_m$$

with

$$\hat{n} \times \{\hat{n} \times \vec{H}(\pm)\} = -R_m \vec{J}_m$$

where  $\vec{J}_m$  is the magnetic current supported and, the convention followed for the signs is the same as in the resistive sheet case.

Note that an *impedance surface* is a simulation of a thin layer whose permittivity and permeability both differ from the surrounding medium. Therefore, a combined sheet consisting of resistive and conductive ones is equivalent to an impedance surface. Although the two sheets are, in general, coupled, with each affecting the scattering from the other, decoupling occurs when the sheets lie in a plane. It is therefore sufficient to solve the problem for the simpler case of the resistive sheet and use the duality principle to get the solution for the other. The solution of the combination sheet can follow by adding the two solutions [Ref. 1].

## B. REFLECTION AND TRANSMISSION

The reflection and transmission coefficients for a resistive film can be derived from the boundary conditions in Equations (2), (3) and (4) and the geometry shown in Figure 1. The subscripts  $i$ ,  $s$  and  $t$  refer to incident, scattered (or reflected) and transmitted, respectively. The two principal polarizations (parallel and perpendicular) are investigated separately. Specular reflection, and transmission at the angle of incidence is assumed, because the sheet is infinitely thin.

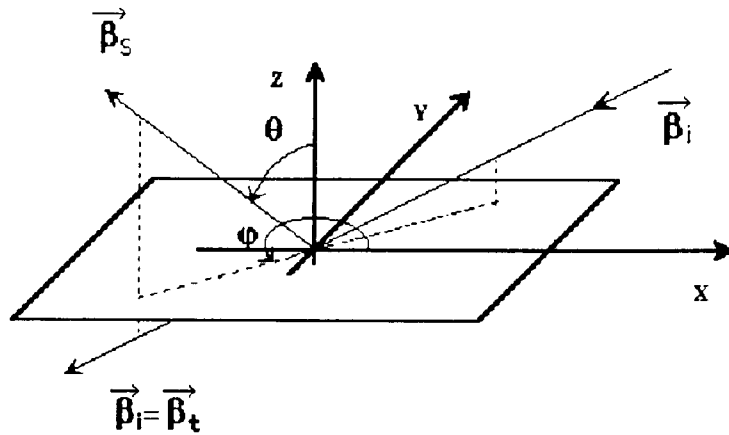


**Figure 1:** Reflection and transmission from a resistive sheet.

### 1. Parallel Polarization

For parallel polarization, the electric field of the incident wave lies in the plane of incidence

$$\vec{E}^i = \theta E_0^i e^{-j\vec{B}_i \cdot \vec{r}}. \quad (5)$$

Without loss of generality, it can be assumed that the plane of incidence is the x-z plane. Figure 2 shows a cut through the  $\phi=0$  plane.

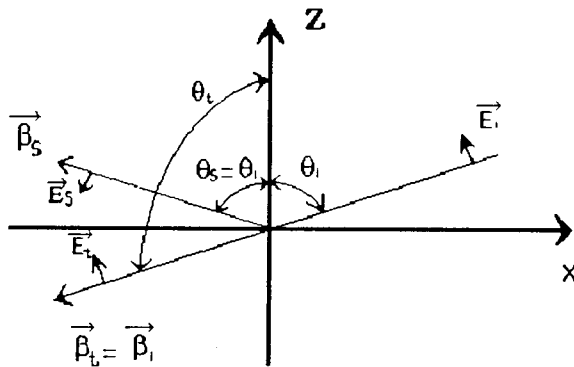


**Figure 2:** A cut of Figure 1 in the plane of incidence.

The incident fields are

$$\vec{E}^i = E_o [-\hat{x}\cos(\theta_i) + \hat{z}\sin(\theta_i)] e^{-j\beta[-x\sin(\theta_i) - z\cos(\theta_i)]} \quad (6)$$

and

$$\vec{H}^i = \hat{y} \frac{E_o}{\eta_o} e^{-j\beta[-x\sin(\theta_i) - z\cos(\theta_i)]} \quad (7)$$

where  $\beta = \frac{2\pi}{\lambda}$  is the wave number. Denoting  $T_p$  as the transmission coefficient for parallel polarization, the transmitted fields are

$$\vec{E}^t = T_p E_o [-\hat{x}\cos(\theta_i) + \hat{z}\sin(\theta_i)] e^{-j\beta[-x\sin(\theta_i) - z\cos(\theta_i)]} \quad (8)$$

and

$$\vec{H}^t = \hat{y} T_p \frac{E_o}{\eta_o} e^{-j\beta[-x\sin(\theta_i) - z\cos(\theta_i)]} \quad (9)$$

Finally the scattered fields are

$$\vec{E}^s = \Gamma_p E_o [-\hat{x}\cos(\theta_i) - \hat{z}\sin(\theta_i)] e^{-j\beta[-x\sin(\theta_i) + z\cos(\theta_i)]} \quad (10)$$

and

$$\vec{H}^s = -\hat{y} \Gamma_p \frac{E_o}{\eta_o} e^{-j\beta[-x\sin(\theta_i) + z\cos(\theta_i)]} \quad (11)$$

where  $\Gamma_p$  is the reflection coefficient for parallel polarization. Using the notation introduced in Section A and applying the boundary conditions on the electric field intensity at  $z=0$

$$\begin{aligned}\vec{E}(+) &= (\vec{E}^i + \vec{E}^s)|_{z=0}, \\ \vec{E}(-) &= \vec{E}^t|_{z=0}.\end{aligned}\tag{12}$$

Similarly for the boundary conditions on the magnetic field intensity

$$\begin{aligned}\vec{H}(+) &= (\vec{H}^i + \vec{H}^s)|_{z=0}, \\ \vec{H}(-) &= \vec{H}^t|_{z=0}.\end{aligned}\tag{13}$$

Inserting Equations (6), (8), (10), and (12) into (2) gives

$$T_p = 1 + \Gamma_p. \tag{14}$$

Using Equations (7), (9), (11) and (13) into (3) gives

$$\vec{J}_s = -\hat{x} \frac{E_o}{\eta_o} (1 - \Gamma_p - T_p) e^{-j\beta[-x \sin(\theta_i)]}. \tag{15}$$

Using Equation (4) and Equation (15)

$$T_p \cos(\theta_i) = \frac{R_s}{\eta_o} (1 - \Gamma_p - T_p). \tag{16}$$

Solving Equations (14) and (16) for the reflection coefficient yields

$$\Gamma_p = \frac{-\eta_o \cos(\theta_i)}{2R_s + \eta_o \cos(\theta_i)}. \tag{17}$$

and for the transmission coefficient

$$T_p = \frac{2R_s}{2R_s + \eta_o \cos(\theta_i)}. \tag{18}$$

## 2. Perpendicular (Normal) Polarization

For perpendicular polarization a similar procedure is followed for deriving the reflection and transmission coefficients. In general the incident field is of the form

$$\vec{E}^i = \hat{\Phi} E_o e^{-j\beta_i \vec{r}_i}. \quad (19)$$

Again, without loss of generality, the x-z plane is considered as the plane of incidence. Expressions for the incident waves are

$$\vec{E}^i = -\hat{y} E_o e^{-j\beta [-x\sin(\theta_i) - z\cos(\theta_i)]}, \quad (20)$$

$$\vec{H}^i = \frac{E_o}{\eta_o} [-\hat{x}\cos(\theta_i) + \hat{z}\sin(\theta_i)] e^{-j\beta [-x\sin(\theta_i) - z\cos(\theta_i)]}. \quad (21)$$

Denoting  $T_n$  and  $\Gamma_n$  the transmission and reflection coefficients respectively for normal polarization, the scattered and transmitted fields are

$$\vec{E}^t = -\hat{y} T_n E_o e^{-j\beta [-x\sin(\theta_i) - z\cos(\theta_i)]}, \quad (22)$$

$$\vec{H}^t = T_n \frac{E_o}{\eta_o} [-\hat{x}\cos(\theta_i) + \hat{z}\sin(\theta_i)] e^{-j\beta [-x\sin(\theta_i) - z\cos(\theta_i)]}, \quad (23)$$

$$\vec{E}^s = -\hat{y} \Gamma_n E_o e^{-j\beta [-x\sin(\theta_i) + z\cos(\theta_i)]}, \quad (24)$$

and

$$\vec{H}^s = \Gamma_n \frac{E_o}{\eta_o} [\hat{x} \cos(\theta_i) + \hat{z} \sin(\theta_i)] e^{-j\beta [-x \sin(\theta_i) + z \cos(\theta_i)]}. \quad (25)$$

Applying Equations (20), (22), (24) and (12) to (2) gives

$$T_n = 1 + \Gamma_n. \quad (26)$$

To obtain the surface current, Equations (21), (23), (25) and (13) are inserted into (2) yielding

$$\vec{J}_s = \hat{y} \frac{E_o}{\eta_o} \cos(\theta_i) (\Gamma_n + T_n - 1) e^{-j\beta [-x \sin(\theta_i)]}. \quad (27)$$

Using Equation (27) in the boundary condition (Equation (3)) gives

$$T_n = \frac{R_s}{\eta_o} \cos(\theta_i) (1 - T_n - \Gamma_n). \quad (28)$$

Solving Equations (26) and (28) for the reflection and transmission coefficients gives

$$\Gamma_n = \frac{-\eta_o}{2R_s \cos(\theta_i) + \eta_o} \quad (29)$$

and

$$T_n = \frac{2R_s \cos(\theta_i)}{2R_s \cos(\theta_i) + \eta_o}. \quad (30)$$

### C. RADIATION AND SCATTERING EQUATIONS

In general, electric and magnetic currents are the sources of radiated or scattered fields. For the case of a resistive sheet the magnetic currents are zero. The formulas simplify further when only the far zone fields are of interest.

The formulas for the far - field calculation are derived by Balanis [Ref. 5] and are given in this section for the reader's convenience. They are specified for the case of currents in the x-y plane of a Cartesian coordinate system as shown in Figure 3.

The spherical components of the electric field intensity are

$$E_r \approx 0 ,$$

$$E_\theta = - \frac{j\beta e^{-j\beta r}}{4\pi r} \eta_o N_\theta , \quad (31)$$

$$E_\phi = - \frac{j\beta e^{-j\beta r}}{4\pi r} \eta_o N_\phi , \quad (32)$$

where

$$N_\theta = \iint_s [J_x \cos(\theta) \cos(\phi) + J_y \cos(\theta) \sin(\phi)] e^{j\beta r' \cos\psi} dx' dy' \quad (33)$$

$$N_\phi = \iint_s [-J_x \sin(\phi) + J_y \cos(\phi)] e^{j\beta r' \cos\psi} dx' dy' , \quad (34)$$

and

$$r' \cos\psi = x' \sin(\theta) \cos(\phi) + y' \sin(\theta) \sin(\phi) = x' u + y' v = g . \quad (35)$$

For the observation point appearing in Equation (35) the direction cosines are defined by

$$\begin{aligned} u &= \sin(\theta) \cos(\phi) , \\ v &= \sin(\theta) \sin(\phi) , \\ w &= \cos(\theta) . \end{aligned} \quad (36)$$

In Chapter III the currents derived in Section B will be

used in the radiation integrals (Equations (31) and (32)) to obtain the scattered fields. The currents are functions of the surface resistivity through the reflection (or transmission) coefficients. Thus, for the synthesis problem  $E_\theta$  and  $E_\phi$  in Equations (31) and (32) are known but, the currents  $J_x$  and  $J_y$  (functions of  $R_s$ ) are unknown.

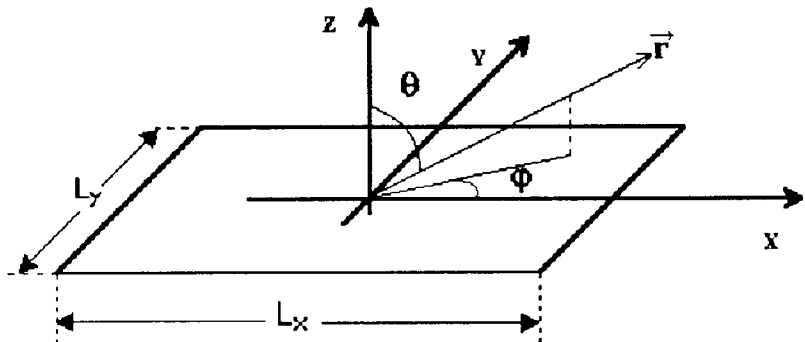


**Figure 3:** Coordinate system for scattering from a planar rectangular plate.

All the formulas assume that the current is not affected by the presence of the edge. This turns out to be a valid assumption for resistive surfaces of finite size because the edges are "softer" than perfectly conducting edges.

### III. FORMULATION AND SOLUTION

The scattering from a planar rectangular resistive sheet with surface resistivity  $R_s$  is investigated for the monostatic and bistatic cases. Using Equation (4), an estimate for the current distribution is obtained, and the total scattered field is calculated. To verify the synthesis equations, the calculated field is used to initiate the synthesis procedure for the surface resistance.

The geometry under consideration is still that shown in Figure 1. The sheet lies in the x-y plane and is illuminated by a plane wave whose electric field contains both parallel and perpendicular components

$$\vec{E}^i = (\hat{\theta} E_\theta^i + \hat{\phi} E_\phi^i) e^{-j\vec{\beta}_i \cdot \vec{r}} \quad (37)$$

where

$$\begin{aligned} -j\vec{\beta}_i \cdot \vec{r} &= j\beta [x \sin(\theta_i) \cos(\phi_i) + y \sin(\theta_i) \sin(\phi_i) + z \cos(\theta_i)] \\ &= j\beta [x u_i + y v_i + z w_i]. \end{aligned}$$

On the surface of the sheet ( $z=0$  and  $\vec{r}=\vec{r}'$ )

$$-j\vec{\beta}_i \cdot \vec{r} = -j\vec{\beta}_i \cdot \vec{r}' = j\beta (x' u_i + y' v_i) \equiv j\beta h. \quad (38)$$

The formulation as well as the analysis of the problem is different for the bistatic and monostatic cases and, therefore, each is considered separately.

#### A. BISTATIC CASE

Equation (4) with  $\hat{n}=\hat{z}$  becomes

$$\hat{z} \times (\hat{z} \times \vec{E}(-)) = -R_s \vec{J}_s \quad (39)$$

where

$$\vec{E}(-) = \vec{E}^t = (\theta T_p E_\theta^i + \phi T_n E_\phi^i) e^{j\beta h}. \quad (40)$$

The cross products are

$$\hat{z} \times \hat{\theta} = -\hat{x} \cos(\theta) \sin(\phi) + \hat{y} \cos(\theta) \cos(\phi)$$

$$\hat{z} \times \hat{\phi} = -\hat{x} \cos(\phi) - \hat{y} \sin(\phi)$$

and the triple products

$$\hat{z} \times (\hat{z} \times \hat{\theta}) = -(\hat{x} \cos(\theta) \cos(\phi) + \hat{y} \cos(\theta) \sin(\phi))$$

and

$$\hat{z} \times (\hat{z} \times \hat{\phi}) = \hat{x} \sin(\phi) - \hat{y} \cos(\phi).$$

Then

$$\begin{aligned} \hat{z} \times (\hat{z} \times \vec{E}(-)) &= \{-\hat{x} [\cos(\theta_i) \cos(\phi_i) T_p E_\theta^i - \sin(\phi_i) T_n E_\phi^i] \\ &\quad - \hat{y} [\cos(\theta_i) \sin(\phi_i) T_p E_\theta^i + \cos(\phi_i) T_n E_\phi^i]\} e^{j\beta h}. \end{aligned}$$

Substituting in the explicit expressions for the transmission coefficients (Equations (18) and (30)), into (40), Equation (39) gives the components of the current on the surface of the sheet

$$J_x = 2 \left( \frac{\cos(\theta_i) \cos(\phi_i) E_\theta^i}{2R_s + \eta_o \cos(\theta_i)} - \frac{\sin(\phi_i) \cos(\theta_i) E_\phi^i}{2R_s \cos(\theta_i) + \eta_o} \right) e^{j\beta h}, \quad (41)$$

$$J_y = 2 \left( \frac{\cos(\theta_i) \sin(\phi_i) E_\theta^i}{2R_s + \eta_o \cos(\theta_i)} + \frac{\cos(\phi_i) \cos(\theta_i) E_\phi^i}{2R_s \cos(\theta_i) + \eta_o} \right) e^{j\beta h}. \quad (42)$$

Now that the currents are known, the scattered fields can be calculated. Because of the complexity of the formulas, parallel and perpendicular polarizations are treated separately. Besides, any arbitrary polarization can be decomposed into a sum of these two orthogonal components.

### 1. Parallel Polarization

When the field is parallel polarized  $E_\phi^i = 0$  and Equations (41) and (42) simplify to

$$J_x = 2 E_\theta^i e^{jk\beta h} \cos(\theta_i) \cos(\phi_i) \frac{1}{2R_s + \eta_o \cos(\theta_i)}, \quad (43)$$

$$J_y = 2 E_\theta^i e^{jk\beta h} \cos(\theta_i) \sin(\phi_i) \frac{1}{2R_s + \eta_o \cos(\theta_i)}. \quad (44)$$

Using equations (43) and (44) in (33) gives

$$N_\theta = 2 E_\theta^i \cos(\theta) \cos(\theta_i) \cos(\phi - \phi_i) I_1 \quad (45)$$

where a new quantity has been defined for convenience

$$I_1 = \iint_s \frac{e^{jk(h+g)}}{2R_s + \eta_o \cos(\theta_i)} dx' dy'. \quad (46)$$

The resistivity is a function of position in general and, therefore, it cannot be taken out of the integral. In order to reduce the scattering equations to closed form expressions, it is assumed that the resistivity profile can be accurately represented by a step approximation. The resistivity function is represented by a series of basis functions (pulses) with unknown coefficients

$$R_s(x', y') = \sum_{m=1}^M \sum_{n=1}^N r_{mn} f_{mn}(x', y') \quad (47)$$

where  $M$  and  $N$  are the number of patches in the  $y$  and  $x$  directions respectively. The unknown expansion coefficients are  $\{r_{mn}\}$  and the expansion functions are two-dimensional steps or "pedestals"

$$f_{mn}(x', y') = \begin{cases} 1, & x', y' \in S_{mn}, \\ 0, & \text{else.} \end{cases} \quad (48)$$

The geometry is defined in Figure 4. The center of the  $mn^{\text{th}}$  patch is at  $(x_{mn}, y_{mn})$  and each patch has dimensions  $\Delta x$  by  $\Delta y$ .

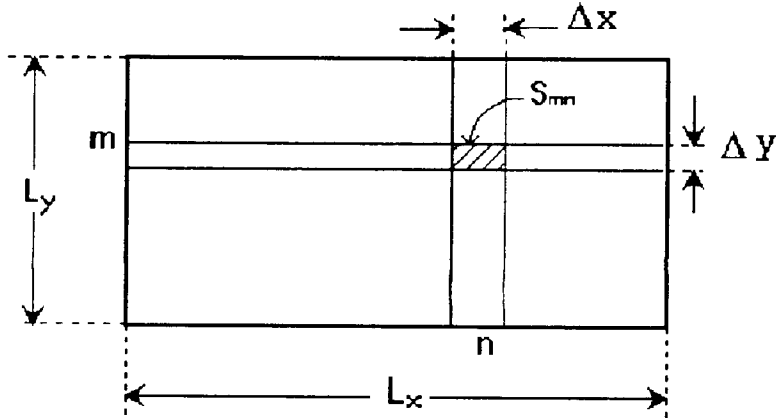


**Figure 4:** Division of the sheet into rectangular subdomains.

Applying the series representation (47) to (46) gives

$$\begin{aligned} I_1 &= \iint_s \frac{e^{j\beta(h+g)}}{2R_s + \eta_o \cos(\theta_i)} dx' dy' \\ &= \iint_s \frac{e^{j\beta(h+g)}}{2 \sum_{m=1}^M \sum_{n=1}^N r_{mn} f_{mn} + \eta_o \cos(\theta_i)} dx' dy' \\ &= \sum_{m=1}^M \sum_{n=1}^N \iint_{S_{mn}} \frac{e^{j\beta(h+g)}}{2r_{mn} + \eta_o \cos(\theta_i)} dx' dy'. \end{aligned}$$

For the  $mn^{\text{th}}$  term of the sum the integral is

$$\begin{aligned} &\iint_{S_{mn}} \frac{e^{j\beta(h+g)}}{2r_{mn} + \eta_o \cos(\theta_i)} dx' dy' = \\ &\frac{1}{2r_{mn} + \eta_o \cos(\theta_i)} \iint_{S_{mn}} e^{jk(h+g)} dx' dy'. \end{aligned} \quad (49)$$

Evaluating the integral in (49) yields a closed form expression in terms of *sinc* functions. Thus  $I_1$  becomes

$$I_1 = \Delta x \Delta y S_u S_v \sum_{m=1}^M \sum_{n=1}^N a_{mn} e^{j\beta P_{mn}} \quad (50)$$

where

$$S_u = \frac{\sin[\beta(u+u_i)\Delta x/2]}{\beta(u+u_i)\Delta x/2} = \text{sinc}[\frac{\beta(u+u_i)\Delta x}{2}], \quad (51)$$

$$S_v = \frac{\sin[\beta(v+v_i)\Delta y/2]}{\beta(v+v_i)\Delta y/2} = \text{sinc}[\frac{\beta(v+v_i)\Delta y}{2}], \quad (52)$$

$$a_{mn} = \frac{1}{2r_{mn} + \eta_o \cos(\theta_i)}, \quad (53)$$

and

$$P_{mn} = x_{mn}(u+u_i) + y_{mn}(v+v_i). \quad (54)$$

Using Equation (50) allows Equation (45) to be written as

$$N_\theta = 2E_\theta^i \cos(\theta_i) \cos(\theta) \cos(\phi - \phi_i) \Delta x \Delta y S_u S_v \sum_{m=1}^M \sum_{n=1}^N a_{mn} e^{j\beta P_{mn}}.$$

Finally, the complete expression of the  $\theta$ -component of the scattered electric field for a parallel polarized incident field is

$$E_{\theta\theta}^s = C_o E_\theta^i \cos(\theta_i) \cos(\theta) \cos(\phi - \phi_i) I_1 \quad (55)$$

where

$$C_o = \frac{-j\beta\eta_o e^{-j\beta r}}{2\pi r} . \quad (56)$$

The first subscript on  $E_{pq}^s$  denotes the polarization of the scattered field, whereas the second subscript denotes the polarization of the incident wave.

By the definition of the radar cross section for a three-dimensional target

$$\sigma = \lim_{r \rightarrow \infty} [4\pi r^2 \frac{|\vec{E}^s|^2}{|\vec{E}^i|^2}] \quad (57)$$

one obtains for this case

$$\sigma_{\theta\theta} = \frac{(\eta_o\beta)^2}{\pi} [\cos(\theta_i) \cos(\theta) \cos(\phi - \phi_i) I_1]^2 \quad (58)$$

To calculate the  $\phi$ -component of the scattered electric field,  $E_{\phi\theta}$ , Equation (32) is used along with Equations (34), (43) and (44). Following the same procedure

$$E_{\phi\theta}^s = -C_o E_\theta^i \cos(\theta_i) \sin(\phi - \phi_i) I_1 \quad (59)$$

and the corresponding radar cross section is

$$\sigma_{\phi\theta} = \frac{(\eta_o\beta)^2}{\pi} [\cos(\theta_i) \sin(\phi - \phi_i) I_1]^2 . \quad (60)$$

## 2. Perpendicular Polarization

When the incident field is normally polarized ( $E_\theta^i = 0$ ), the current components in Equations (41), (42) reduce to

$$J_x = -2 E_\phi^i e^{j\beta h} \sin(\phi_i) \cos(\theta_i) \frac{1}{2R_s \cos(\theta_i) + \eta_o} , \quad (61)$$

$$J_y = 2 E_\phi^i e^{j\beta h} \cos(\phi_i) \cos(\theta_i) \frac{1}{2R_s \cos(\theta_i) + \eta_o}. \quad (62)$$

Using Equations (61) and (62) in (33) gives

$$N_\theta = 2 E_\phi^i \cos(\theta) \cos(\theta_i) \sin(\phi - \phi_i) I_2 \quad (63)$$

where

$$I_2 = \iint_s \frac{e^{jk(h+g)}}{2R_s \cos(\theta_i) + \eta_o} dx' dy'.$$

Following the procedure used for parallel polarization one obtains

$$I_2 = \Delta x \Delta y S_u S_v \sum_{m=1}^M \sum_{n=1}^N b_{mn} e^{j\beta P_{mn}} \quad (64)$$

with

$$b_{mn} = \frac{1}{2r_{mn} \cos(\theta_i) + \eta_o}. \quad (65)$$

Finally, using Equation (63) in (31) gives the  $\theta$ -polarized component of the scattered field

$$E_{\theta\phi}^s = C_o E_\phi^i \cos(\theta) \cos(\theta_i) \sin(\phi - \phi_i) I_2. \quad (66)$$

The corresponding radar cross section is then

$$\sigma_{\theta\phi} = \frac{(\eta_o \beta)^2}{\pi} [\cos(\theta) \cos(\theta_i) \sin(\phi - \phi_i) I_2]^2. \quad (67)$$

To determine the  $\phi$ -component of the scattered field, Equation (34) is used, yielding

$$N_\phi = 2 E_\phi^i \cos(\theta_i) \cos(\phi - \phi_i) I_2$$

and then

$$E_{\phi\phi}^s = C_o E_\phi^i \cos(\theta_i) \cos(\phi - \phi_i) I_2. \quad (68)$$

The corresponding radar cross section is

$$\sigma_{\phi\phi} = \frac{(\eta_o \beta)^2}{\pi} [\cos(\theta_i) \cos(\phi - \phi_i) I_2]^2. \quad (69)$$

### 3. Arbitrary Polarization

In general, the incident wave is composed of both parallel and perpendicular components. Thus it is necessary to combine the results of Subsections 1 and 2. The total  $\theta$  and  $\phi$  components of the scattered field intensity are given by

$$\begin{aligned} E_\theta^S &= E_{\theta\theta}^S + E_{\theta\phi}^S \\ &= C_o \cos(\theta) \cos(\theta_i) [E_\theta^i \cos(\phi - \phi_i) I_1 + E_\phi^i \sin(\phi - \phi_i) I_2] \end{aligned} \quad (70)$$

and

$$\begin{aligned} E_\phi^S &= E_{\phi\theta}^S + E_{\phi\phi}^S \\ &= -C_o \cos(\theta_i) [E_\theta^i \sin(\phi - \phi_i) I_1 - E_\phi^i \cos(\phi - \phi_i) I_2]. \end{aligned} \quad (71)$$

At this point it is possible to cast Equations (70) and (71) in matrix form

$$\begin{bmatrix} E_\theta^S \\ E_\phi^S \end{bmatrix} = \begin{bmatrix} A_{\theta\theta} & A_{\theta\phi} \\ A_{\phi\theta} & A_{\phi\phi} \end{bmatrix} \begin{bmatrix} S_1 \\ S_2 \end{bmatrix} \quad (72)$$

where, using Equations (50) and (64)

$$A_{\theta\theta} = E_\theta^i C_o \Delta x \Delta y \cos(\theta_i) \cos(\theta) \cos(\phi - \phi_i) S_u S_v \quad (73)$$

$$A_{\theta\phi} = E_\phi^i C_o \Delta x \Delta y \cos(\theta_i) \cos(\theta) \sin(\phi - \phi_i) S_u S_v \quad (74)$$

$$A_{\phi\theta} = -E_\theta^i C_o \Delta x \Delta y \cos(\theta_i) \sin(\phi - \phi_i) S_u S_v \quad (75)$$

and

$$A_{\phi\phi} = E_\phi^i C_o \Delta x \Delta y \cos(\theta_i) \cos(\phi - \phi_i) S_u S_v. \quad (76)$$

The terms  $S_1$  and  $S_2$  in the right hand side of Equation (72) represent the double summation terms in (50) and (64) for each scattered field point, namely

$$S_1 = \sum_{m=1}^M \sum_{n=1}^N a_{mn} e^{j\beta P_{mn}} \quad (77)$$

and

$$S_2 = \sum_{m=1}^M \sum_{n=1}^N b_{mn} e^{j\beta P_{mn}}. \quad (78)$$

The resistivity is embedded in the terms  $S_1$  and  $S_2$ .

## B. MONOSTATIC CASE

For the monostatic case ( $\phi = \phi_i$  and  $\theta = \theta_i$ ) and Equations (70) and (71) reduce to

$$E_\theta^s = C_o E_\theta^i \cos^2(\theta) I_1 \quad (79)$$

and

$$E_\phi^s = C_o E_\phi^i \cos(\theta) I_2 \quad (80)$$

respectively. Equation (53) can be written now as

$$a_{mn} = \frac{1}{2 r_{mn} + \eta_o \cos(\theta)} \quad (81)$$

and Equation (65) as

$$b_{mn} = \frac{1}{2r_{mn}\cos(\theta) + \eta_o} . \quad (82)$$

Equations (79) and (80) cannot form a linear system of equations of the form of Equation (72) because the coefficients in vectors  $\underline{a}$  and  $\underline{b}$  (Equations (81) and (82)) change with angle.

The crudest approximation that can be made to eliminate the  $\theta$  dependence is to consider  $\cos(\theta) \approx 1$ . Equations (79) and (80) reduce to

$$E_\theta^s = C_o E_\theta^i I_1 \quad (83)$$

and

$$E_\phi^s = C_o E_\phi^i I_2 \quad (84)$$

and Equations (81) and (82) to

$$a_{mn} = b_{mn} = \frac{1}{2r_{mn} + \eta_o} . \quad (85)$$

The monostatic RCS is for both polarizations

$$\sigma = \frac{(\eta_o \beta)^2}{\pi} I_1^2 . \quad (86)$$

Now it is possible to set up a linear system of equations. In fact, as a  $\theta$ -polarized incident electric field creates only  $\theta$ -polarized scattered electric field, and similarly for a  $\phi$ -polarized incident field, an equation of the form of (72) contains only one component of the scattered field. These equations were implemented in MATLAB and the code listings are given in the Appendix.

### C. SYNTHESIS FORM OF THE SCATTERING EQUATIONS

For RCS synthesis, the scattered field components derived in the two previous sections are known quantities and the expansion coefficients  $\{a_{mn}\}$  and  $\{b_{mn}\}$ , must be determined. Expressing the scattered field equations in appropriate matrix form, it is possible to solve for the expansion coefficients using standard matrix techniques. To achieve this it is convenient to use a single index to count the patches rather than the double summation. Let

$$\sum_{m=1}^M \sum_{n=1}^N c_{mn} e^{j\theta P_{mn}} \rightarrow \sum_{k=1}^{M \times N} c_k e^{j\theta P_k} \quad (87)$$

where  $c_{mn}$  can be either  $a_{mn}$  or  $b_{mn}$ .

There are  $M \times N$  unknowns and therefore  $M \times N$  equations are needed to solve for  $\{a_{mn}\}$  or  $\{b_{mn}\}$ . Because of the periodicity of the *sinc* functions (Equations (51) and (52)) in the direction cosines  $u$  and  $v$ , it is advantageous to work in direction cosine space. As shown in Figure 5, the region defined by  $-1 \leq u, v \leq 1$  is divided into the same number of subsections as there are patches on the sheet. The centers of these subsections  $(u_k, v_k)$  form a grid of points at which the scattered field components are specified, yielding  $M \times N$  values for each field component. The area in the unit circle is the visible region while exterior points have no physical significance.

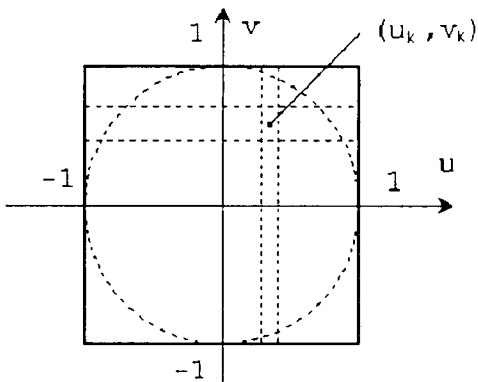


**Figure 5:** Division of direction cosine space into subsections.

The values of  $E_\theta^s$  and  $E_\phi^s$  are used to form a column vector of length  $M \times N$ . Furthermore, at each of the patches,  $\cos(\theta_k)$ ,  $\sin(\phi_k - \phi_i)$ ,  $\cos(\phi_k - \phi_i)$  can be expressed in terms of  $(u_k, v_k)$  according to the following relationships

$$u_k^2 + v_k^2 = \sin^2(\theta_k),$$

$$\frac{v_k}{u_k} = \tan(\phi_k).$$

Inverting these formulas gives

$$\begin{aligned} \cos(\theta_k) &= \sqrt{1 - (u_k^2 + v_k^2)}, \\ \phi_k &= \arctan\left(\frac{v_k}{u_k}\right). \end{aligned} \tag{88}$$

In the direction cosine space the terms  $\cos(\theta)$ ,  $\sin(\phi - \phi_i)$ ,  $\cos(\phi - \phi_i)$  as well as the product  $S_u S_v$  can be written in the form a column vector of length  $M \times N$ . Denoting column vectors with an underline

$$\begin{aligned}
[\underline{X}_1]_k &= \cos(\theta_k), \\
[\underline{X}_2]_k &= \cos(\phi_k - \phi_i), \\
[\underline{X}_3]_k &= \sin(\phi_k - \phi_i), \\
[\underline{X}_4]_k &= S_u(u_k) S_v(v_k).
\end{aligned} \tag{89}$$

We can further define the column vectors  $\underline{X}_a$  and  $\underline{X}_b$  as

$$[\underline{X}_a]_k = \sum_{v=1}^{M \times N} a_v e^{j \beta P_v(u_k, v_k)} \tag{90}$$

and

$$[\underline{X}_b]_k = \sum_{v=1}^{M \times N} b_v e^{j \beta P_v(u_k, v_k)}. \tag{91}$$

The vectors  $\underline{X}_a$  and  $\underline{X}_b$  can also be written as

$$\underline{X}_a = B \underline{a} \tag{92}$$

and

$$\underline{X}_b = B \underline{b} \tag{93}$$

where  $\underline{a}$  and  $\underline{b}$  are column vectors of length  $M \times N$  and follow from equations (53) and (65) respectively. The matrix  $B$  has dimensions  $(M \times N)$  by  $(M \times N)$  and is defined as

$$[B]_{kv} = e^{j \beta [x_v(u_k + u_i) + y_v(v_k + v_i)]} \tag{94}$$

where  $k, v = 1, \dots, M \times N$ .

With the above matrices defined, Equation (70) can be written as

$$\underline{E}_\theta^s = C_1 \cos(\theta_i) \underline{X}_1 * \underline{X}_4 (E_\theta^i \underline{X}_2 * \underline{X}_a + E_\phi^i \underline{X}_3 * \underline{X}_b) \quad (95)$$

where  $*$  denotes an elementwise product and  $C_1 = C_o \Delta x \Delta y$ . Equation (71) becomes

$$\underline{E}_\phi^s = -C_1 \cos(\theta_i) \underline{X}_4 * (E_\theta^i \underline{X}_3 * \underline{X}_a - E_\phi^i \underline{X}_2 * \underline{X}_b). \quad (96)$$

For the monostatic case  $\underline{X}_a = \underline{X}_b = \underline{X}$  and Equation (83) becomes

$$\underline{E}_\theta^s = C_1 E_\theta^i \underline{X}_4 * \underline{X} \quad (97)$$

and Equation (84)

$$\underline{E}_\phi^s = C_1 E_\phi^i \underline{X}_4 * \underline{X}. \quad (98)$$

For this case  $u_i = u$  and  $v_i = v$ , and the matrix  $B$  is defined now as

$$[B]_{kv} = e^{2j\beta[x_v u_k + y_v v_k]} \quad (99)$$

In all of these equations the goal is to solve for the vectors  $\underline{X}_a$ ,  $\underline{X}_b$  or  $\underline{X}$ , which can easily be done using elementwise division. Once these vectors are known, it is possible to solve for  $\underline{a}$  or  $\underline{b}$  of Equations (92) and (93).

## IV. COMPUTER IMPLEMENTATION AND DATA ANALYSIS

### A. GENERAL APPROACH

In this chapter the surface resistivity synthesis procedure is simulated and computational accuracy issues are discussed. The simulation consists of computing the RCS (or scattered fields) of a rectangular sheet with known resistivity. Then the computed RCS is used in the synthesis equations to obtain the resistivity function. In principal, the synthesized distribution should be exactly the same as the original distribution used to compute the RCS. However, in practice, the agreement between the two depends on several factors, such as the sampling method used to fill the vectors  $\underline{E}_\theta^s$  and  $\underline{E}_\phi^s$  in Equations (95) through (98).

From the field equations in matrix form, the scattered field components can be computed in any direction ( $\theta, \phi$ ) when the resistivity function  $R_s$  is defined. To form the vectors  $\underline{E}_\theta^s$  and  $\underline{E}_\phi^s$ ,  $M \times N$  directions must be chosen to compute specific values. Once the vectors  $\underline{E}_\theta^s$  and  $\underline{E}_\phi^s$  are defined, it is possible to solve these equations for the vectors  $\underline{X}_a$ ,  $\underline{X}_b$ , and  $\underline{X}$ . The final step in the synthesis procedure is the reconstruction of the expansion coefficients  $\{r_{mn}\}$  from these vectors.

One approach to choosing the observation directions is to define  $M \times N$  points in direction cosine space as described in Chapter III-C and Figure 5. The square region defined by  $-1 \leq u, v \leq 1$  is divided into patches and their centers represent the chosen directions. Equally spaced points in  $u$  and  $v$  have been used in most calculations, but the spacings in these two principal axes can be different in general. The advantage of this approach is that equal sample spacings work well with scattering patterns that are periodic in  $u$  and  $v$ .

At this point, two variations have been investigated. They are referred to as method (I) and method (II). In method (I) the observation points are restricted to be inside of the

unit circle (visible region), which makes physical sense. A disadvantage of this method is the necessity of forcing the number of patches on the sheet to be equal to the number of sample points in the visible part of direction cosine space. This condition becomes very restrictive as the spacing in  $u$  and  $v$  gets close. Consequently, if  $M \times N$  points are to be contained in the unit circle, the  $-1 \leq u, v \leq 1$  region has to be divided into more than  $M \times N$  patches, say  $N_u$  by  $N_v$ . However, despite this restriction, the method was successful, even for large sizes of the sheet.

A modified version of this approach is method (II) in which the  $M \times N$  direction cosine samples are spread over the complete range  $-1 \leq u, v \leq 1$ . For this case  $N_u = N$  and  $N_v = M$ . Note that the points outside the unit circle are not in the visible region and therefore one might expect that these values would not affect the synthesis result. However, an attempt to set the exterior points equal to zero results in a badly scaled matrix for the fields, and the matrix is almost always impossible to invert. The reason is that setting the exterior field values to zero is an attempt to synthesize a resistivity distribution for a discontinuous pattern. Realizable resistivity functions do not yield scattering patterns that abruptly go to zero. To avoid this problem the calculation can be extended to the exterior points using complex angles. In this case the expression

$$\cos(\theta_k) = \sqrt{1 - (u_k^2 + v_k^2)} \quad (100)$$

can take on complex values. At the corners  $|u_k| = |v_k| = 1$  and,

$$\begin{aligned} |\cos(\theta_k)| &= 1 \\ \arg(\cos(\theta_k)) &= \pm \frac{\pi}{2}. \end{aligned} \quad (101)$$

While the first method makes more physical sense, the

second is more flexible in choosing the number of far-field points (or patches), and is shown to work well over a large range of values of M and N.

To verify the synthesis procedure, the scattered field is calculated using two different resistivity profiles: (i) a constant resistivity ( $R_s=377\Omega$ ) and (ii) a two-dimensional linear taper given by the equation

$$R_s(x, y) = 150(|x| + |y|) \Omega. \quad (102)$$

For the field calculation, a large enough number of patches is used to sufficiently approximate the linear shape of Equation (102). The synthesis was tested using a few specific field points in the range of 9 to 256. This corresponds to M and N in the range of 3 to 16. Beyond that, the method still works well, but computational time increases significantly. Roundoff errors and numerical instability also affect the solution. Matrix B in Equations (92) or (93) has to be inverted and is, in general, an ill-conditioned matrix. It becomes singular as the number of patches increases. In such cases the use of the Moore-Penrose pseudoinverse matrix [Ref. 7] rather than the inverse, was found to give satisfactory results for larger numbers of patches.

## B. BISTATIC CASE

Methods (I) and (II) are applied for the bistatic case, first for a pure  $TM_z$  incident wave, and then for arbitrary incident wave polarization, which is the most general situation. For each resistivity function, the scattered fields are computed for sheets of sizes  $1\lambda \times 1\lambda$  and  $5\lambda \times 5\lambda$ . Data are presented for various numbers of patches and the two resistivity profiles. The plot of the expansion coefficients  $\{r_{mn}\}$  (i.e., the resistivity profile used to calculate the scattered fields) is compared with the reconstructed

resistivity function. For small number of patches, the reconstruction is exact (one can not distinguish them when the plots are overlaid). But as the number of patches increases some numerical and sampling errors can be observed. In general both methods (I) and (II) work well in the entire range of synthesis parameters investigated.

### 1. Parallel Polarization

Assume the incident wave is  $\text{TM}_z$  polarized ( $E_\phi^i = 0$ ) and that it arrives incident from the direction  $\theta_i = 30^\circ$  and  $\phi_i = 0^\circ$ . As an example, the RCS pattern for a one wavelength square sheet is shown in Figure 6. The field has been computed using method (II) and  $N_u = N_v = 64$ . Various synthesis results are presented in Figures 7 through 17. Note that

1.  $M$  and  $N$  are the number of subdivisions on the resistive sheet in the directions  $y$  and  $x$  (see Figure 4).
2.  $N_u$  and  $N_v$  are the number of subdivisions of the region  $-1 \leq u, v \leq 1$  (see Figure 5).
3.  $L_x$  and  $L_y$  are the dimensions of the sheet in  $x$  and  $y$  directions expressed in wavelengths.

It should be noted that in method (I)  $N_u \times N_v \geq M \times N$ , while in method (II)  $N_u = N$  and  $N_v = M$ . In most cases the two methods gave identical results, thus the data will only be presented once.

In Figures 7 and 8, only 16 field points are used with constant and linear taper resistivities. The initial and synthesized distributions are identical. Figure 9 and 10 show that the synthesized linear taper resistivity has a maximum error of 1% when 256 points are used. The relative error for the constant resistivity case with the same number of points becomes 2% as shown in Figure 11.

The RCS for the  $5\lambda \times 5\lambda$  sheet is shown in Figure 12. Again the two resistivity functions are considered. In Figures 13

(constant resistivity) and 14 (linear taper), only 16 field points are needed to recover the exact resistivity function. In Figures 15 through 17 it is seen that the error in the synthesized resistivity is also negligible when 256 points are used. It was found that for a sheet with dimensions  $k\lambda \times k\lambda$ , the choice of  $N_u = N_v = k$  gives converged results.

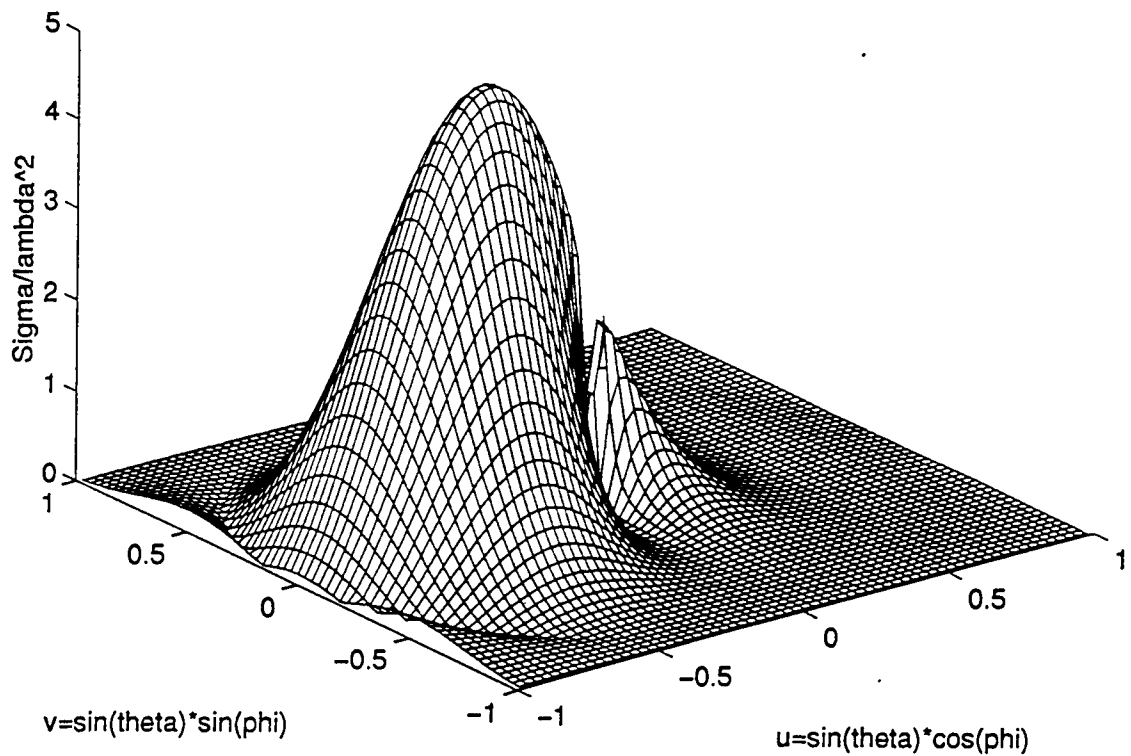


**Figure 6:** Bistatic RCS of a resistive sheet with  $L_x=L_y=\lambda$ ,  $N_u=N_v=64$ ,  $\theta_i=30$  deg,  $\phi_i=0$  deg,  $R_s$  is given by Equation (102).

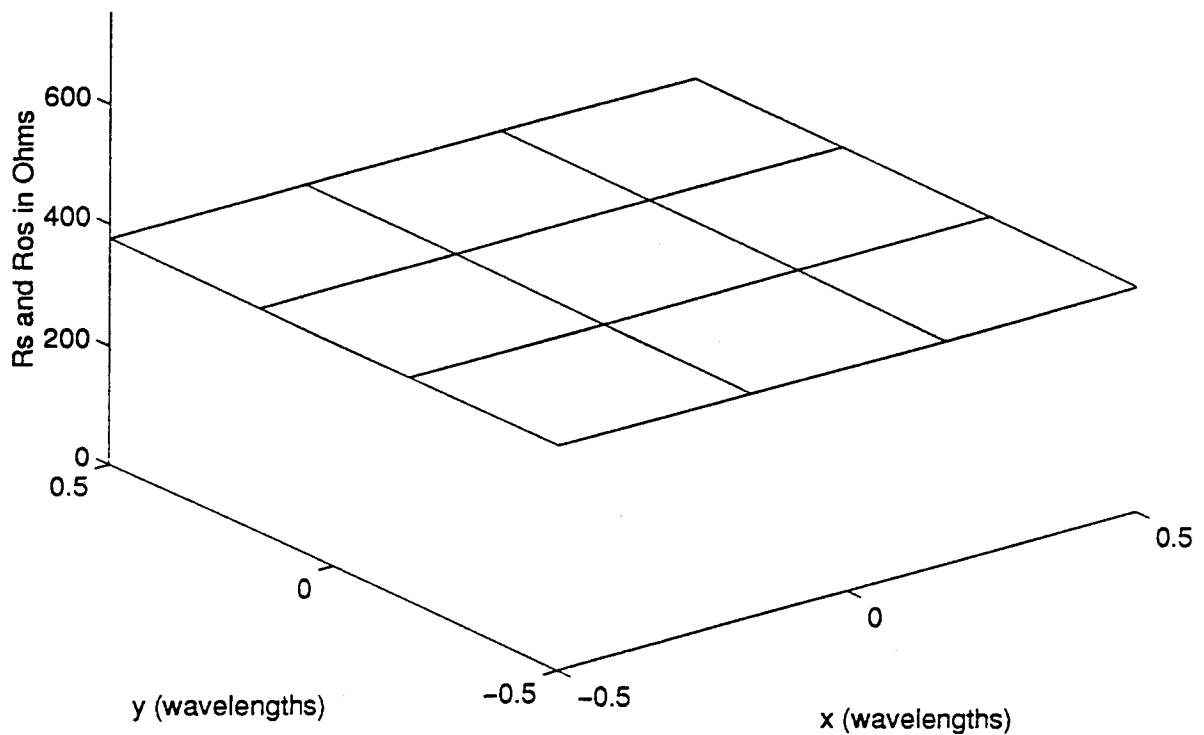


**Figure 7:** Original and synthesized resistivity with method (I) are identical for this case.  $L_x=L_y=\lambda$ ,  $M=N=4$ ,  $N_u=4$ ,  $N_v=5$ .

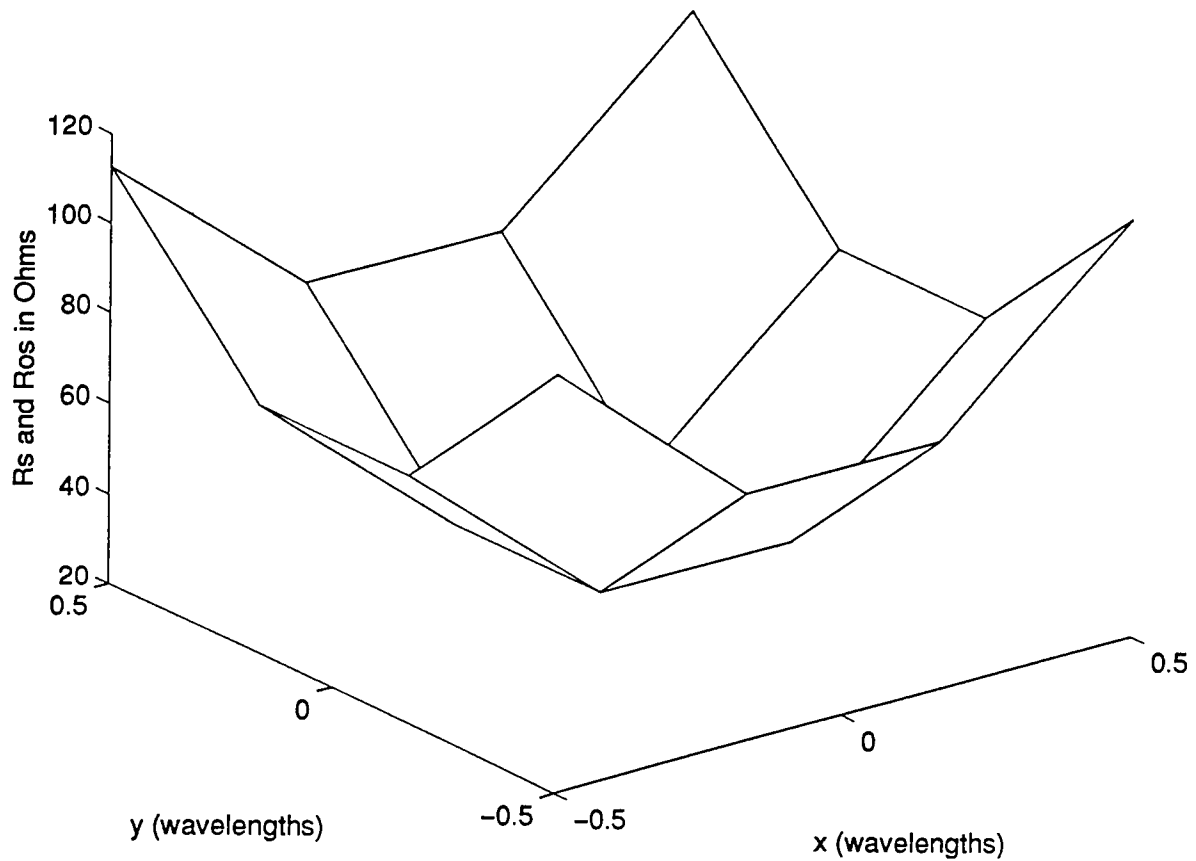


**Figure 8:** Reconstructed and original resistivity functions are identical. For this case  $L_x=L_y=\lambda$ ,  $M=N=4$ ,  $N_u=N_v=4$ .

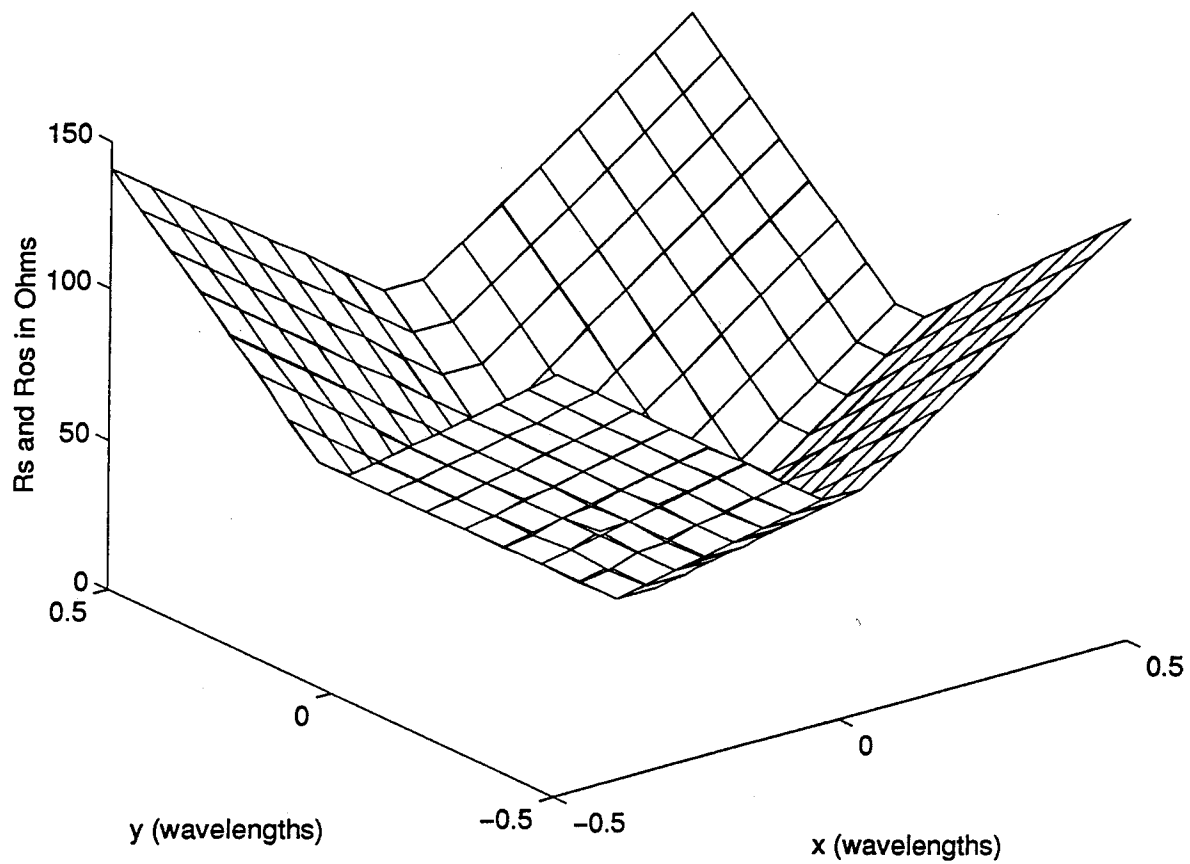


**Figure 9:** Synthesized and original resistivity for  $L_x=L_y=\lambda$ ,  $N=M=16$ ,  $N_u=N_v=16$ . The maximum error is 1%.

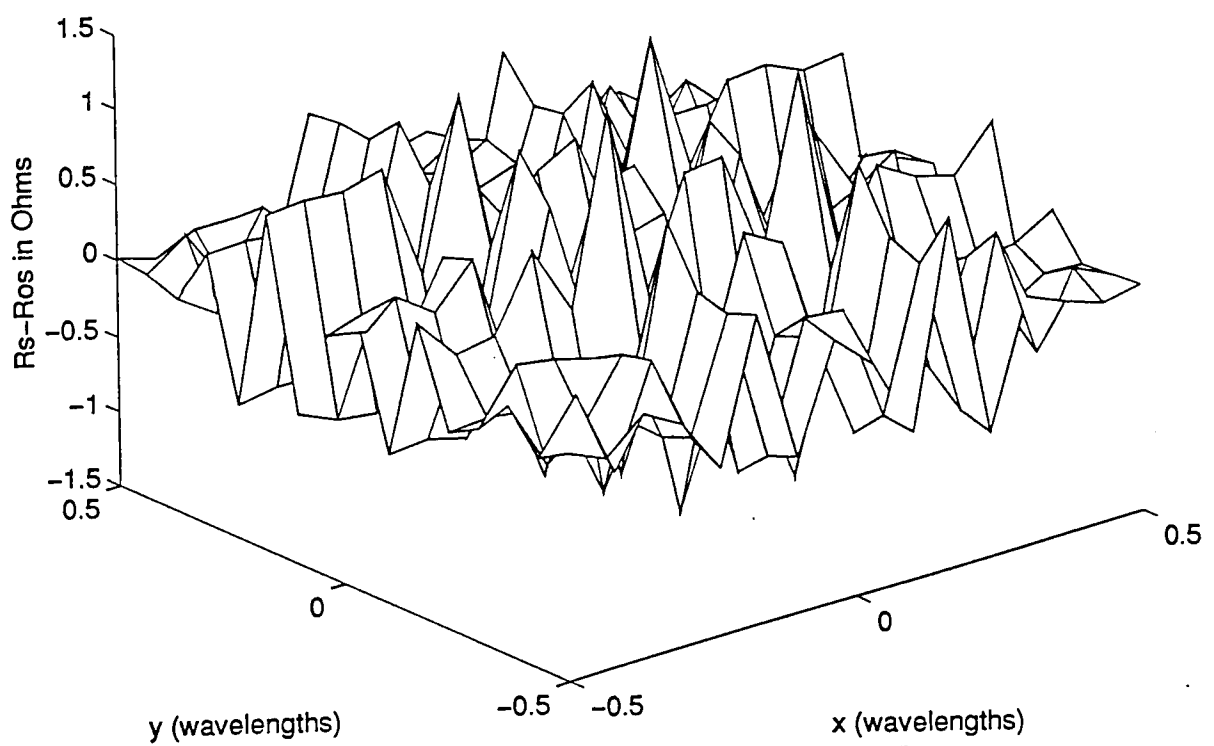


**Figure 10:** Difference of the synthesized and original resistivities shown in Figure 9.

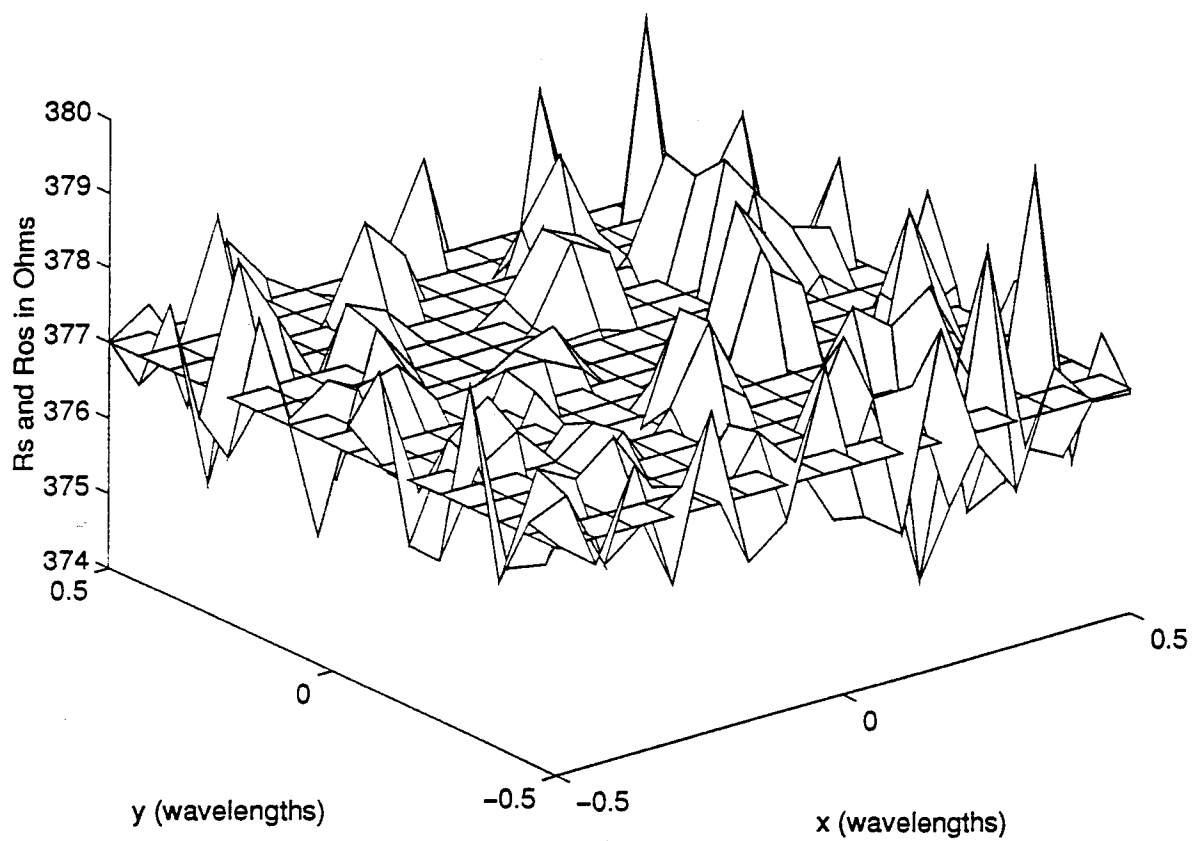


**Figure 11:** Synthesized and original resistivities. For this case,  $L_x=L_y=\lambda$ ,  $M=N=16$  and  $N_u=N_v=16$ . The error is 2%.

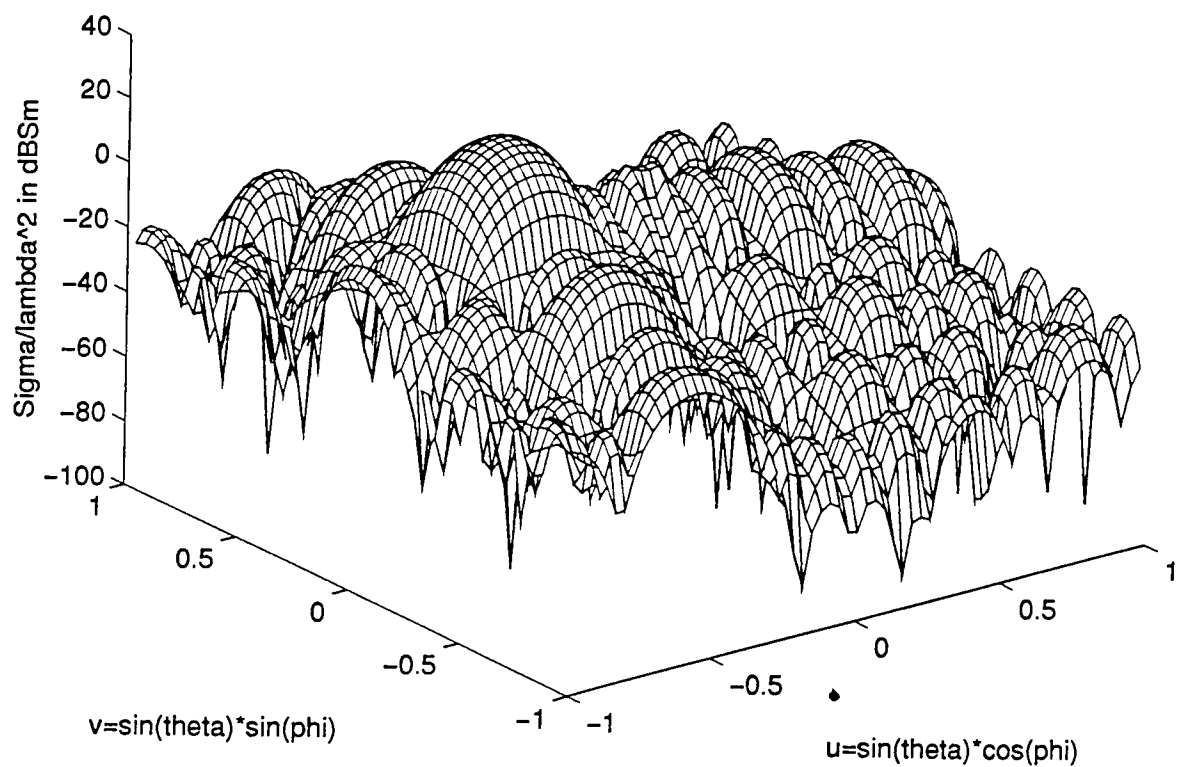


**Figure 12:** Scattered RCS from a resistive sheet.  $R_s$  is given by Equation (102). For this case  $L_x=L_y=5\lambda$ ,  $M=N=64$ ,  $N_u=N_v=64$ ,  $\theta_i=30$  deg,  $\phi_i=0$  deg.

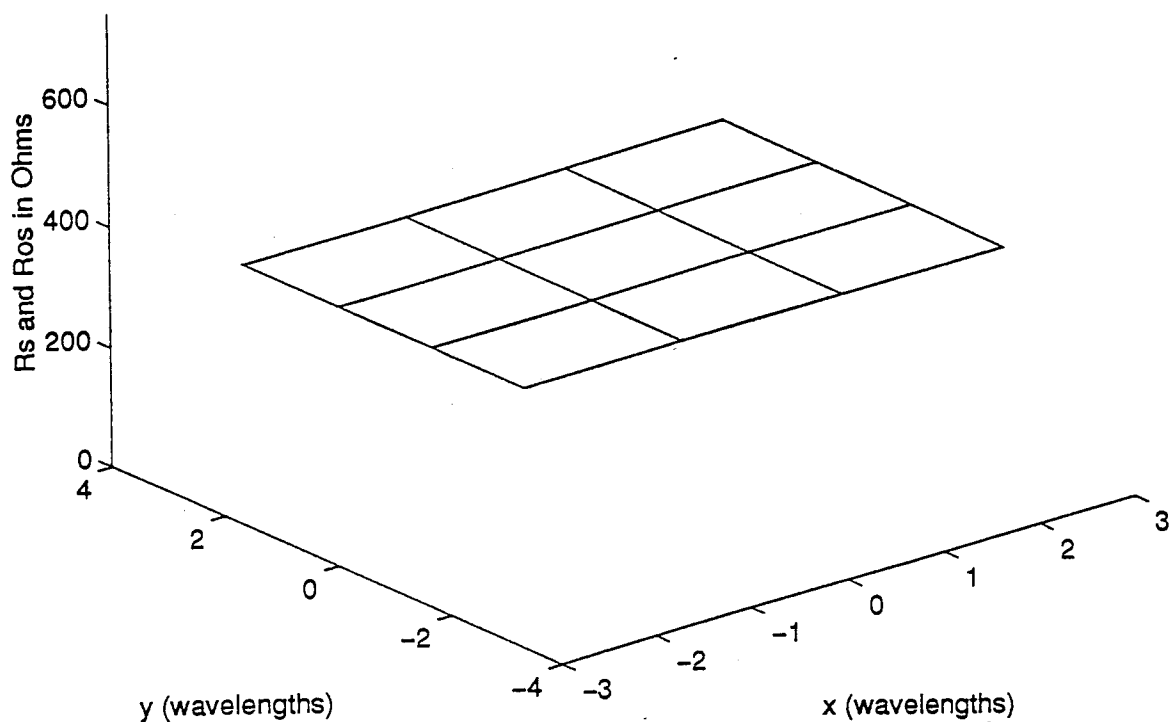


**Figure 13:** Synthesized and original resistivity are identical. For this case,  $Lx=Ly=5\lambda$ ,  $M=N=4$ ,  $N_u=4$ ,  $N_v=5$ .

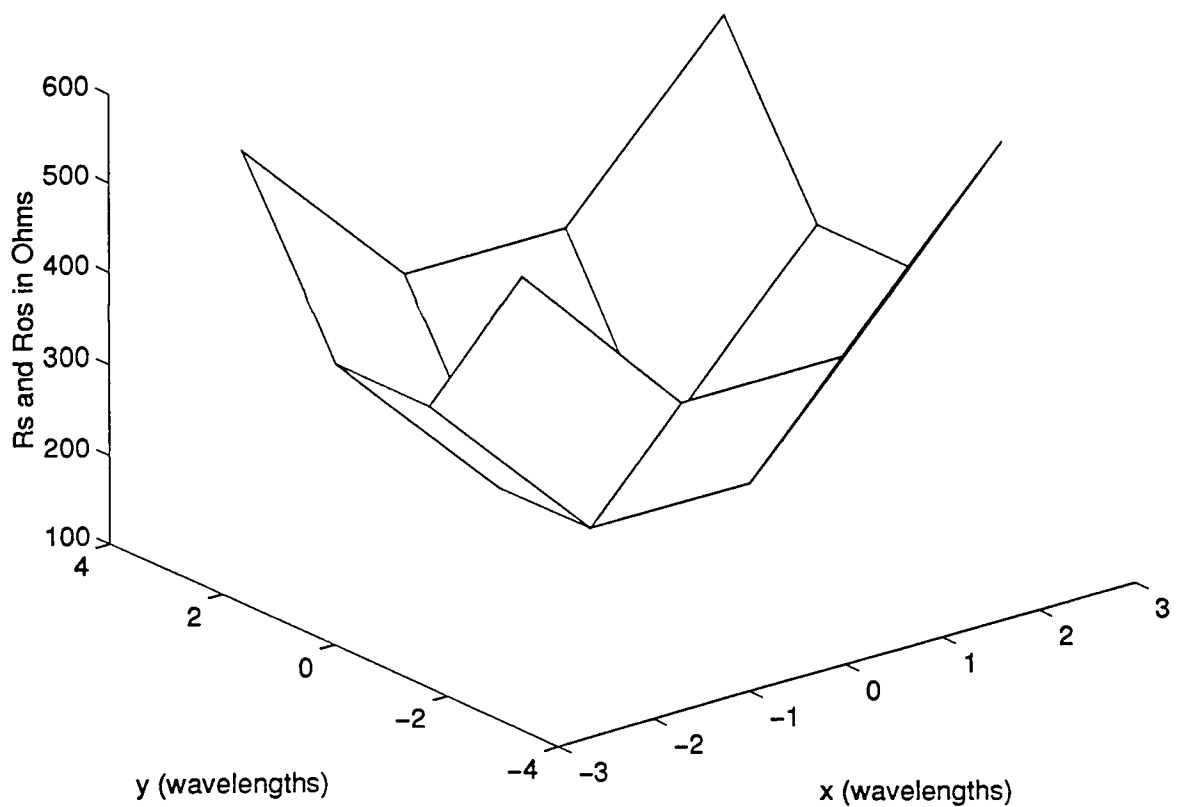


**Figure 14:** Synthesized and original resistivity are identical. For this case,  $L_x=L_y=5\lambda$ ,  $M=N=4$ ,  $N_u=N_v=4$ .

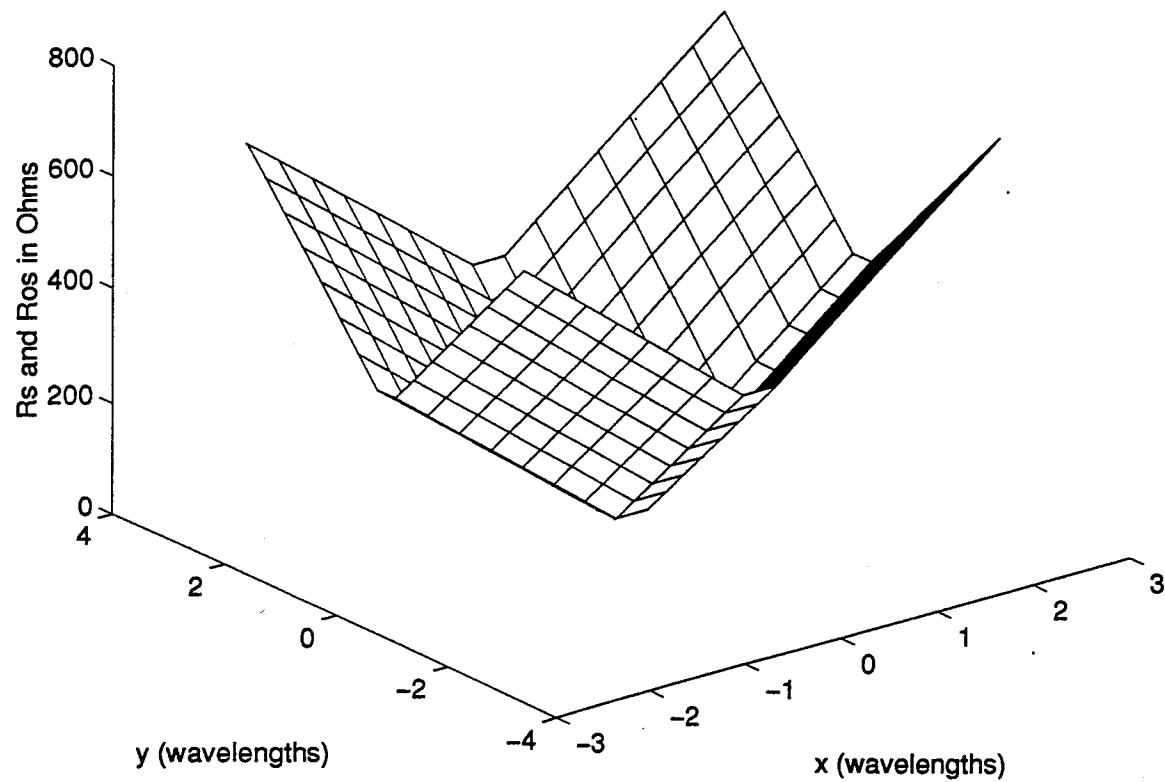


**Figure 15:** Synthesized and original resistivity. For this case,  $L_x=L_y=5\lambda$ ,  $M=N=16$ ,  $N_u=N_v=16$ .

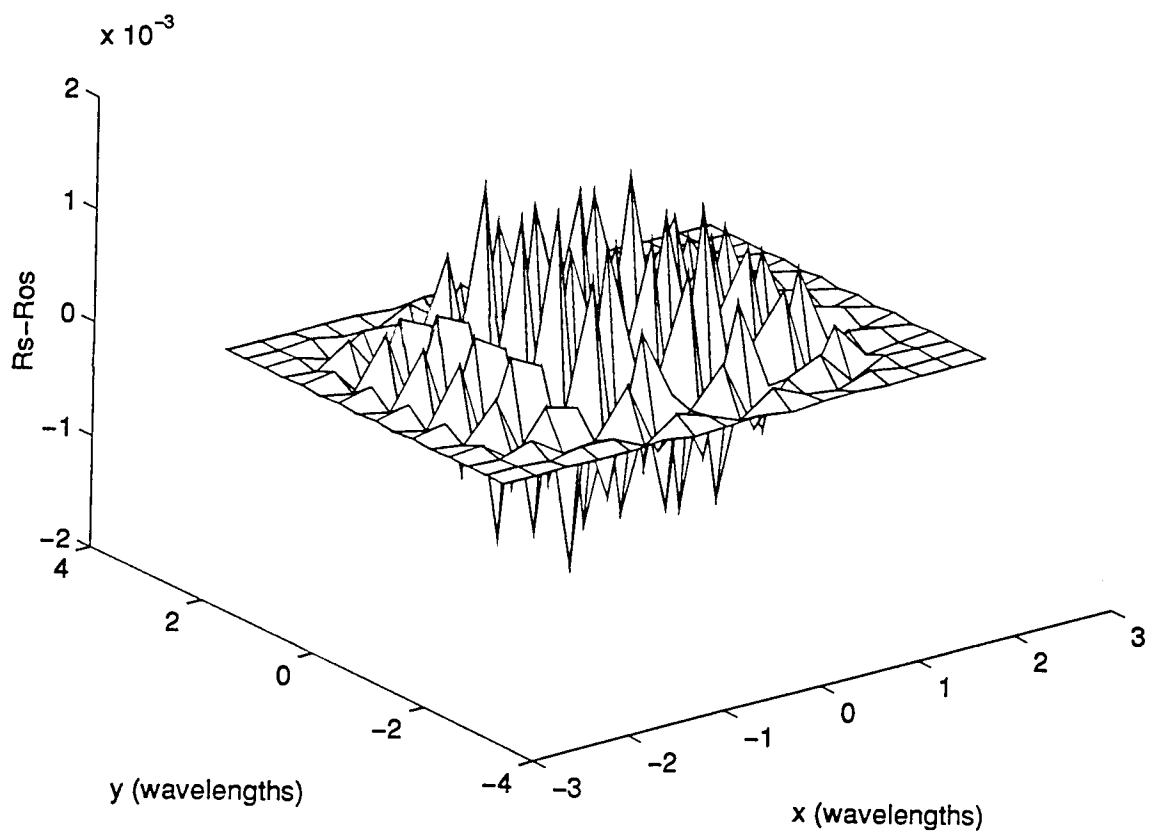


**Figure 16:** Difference of the reconstructed and the original resistivity distribution. The relative error is negligible.

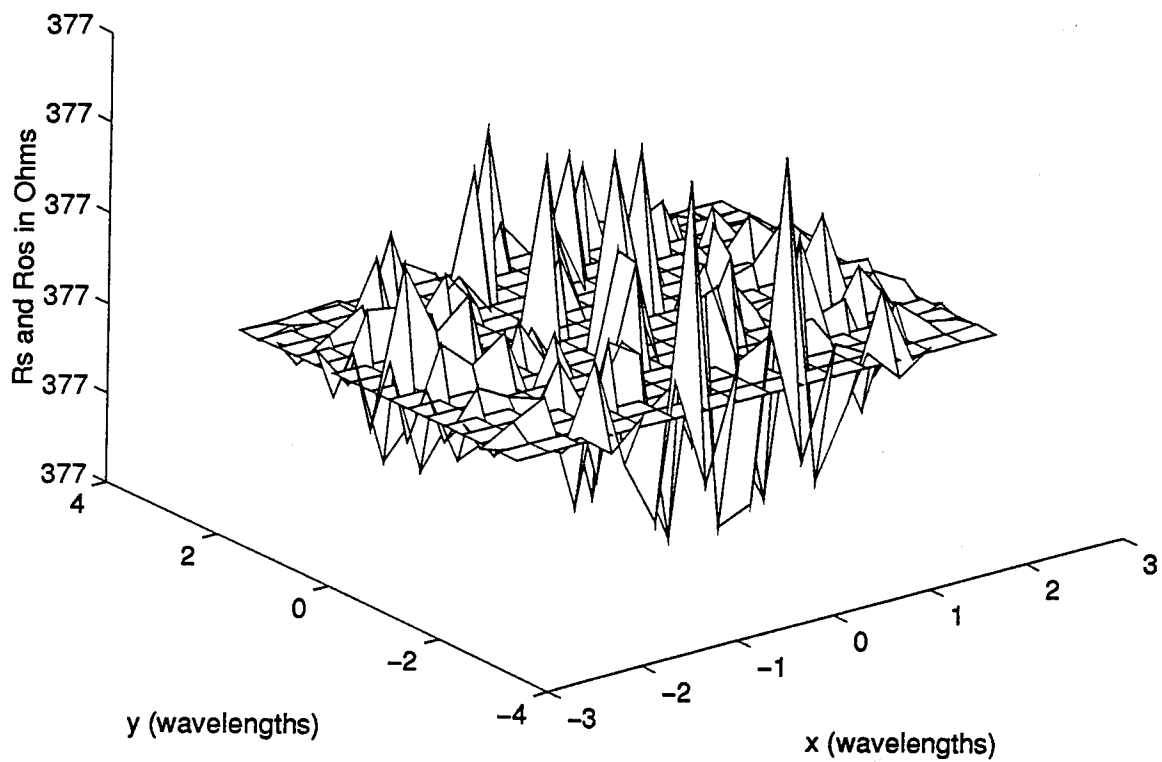


**Figure 17:** Original and synthesized resistivity. For this case,  $L_x=L_y=5\lambda$ ,  $M=N=16$ ,  $N_u=N_v=18$ . The error is negligible.

## 2. Arbitrary Polarization

For the general case where the incident field has both parallel and perpendicular components, both the  $\underline{E}_\theta^s$  and the  $\underline{E}_\phi^s$  vectors given by Equations (95) and (96) depend on  $\underline{X}_a$  and  $\underline{X}_b$ . The vectors  $\underline{X}_a$  and  $\underline{X}_b$  are not independent and both implicitly contain the expansion coefficients  $\{r_{mn}\}$ . An expression of these equations in such a form that permits the solution for  $\{r_{mn}\}$  once the field vectors are known is desired. One approach is to specify the magnitude of the total scattered field as given by

$$\underline{E}^s = \sqrt{|\underline{E}_\theta^s|^2 + |\underline{E}_\phi^s|^2}$$

but this leads to very complicated functions of  $a$  and  $b$ . Alternately, Equations (95) and (96) can be expressed as

$$\begin{aligned} \underline{E}_\theta^s &= A_{\theta\theta} * \underline{S}_1 + A_{\theta\phi} * \underline{S}_2 \\ \underline{E}_\phi^s &= A_{\phi\theta} * \underline{S}_1 + A_{\phi\phi} * \underline{S}_2. \end{aligned} \quad (103)$$

Solving this system for  $\underline{X}_a$  and  $\underline{X}_b$  yields

$$[\underline{X}_a]_i = \frac{[A_{\theta\phi} * \underline{E}_\phi^s - A_{\phi\phi} * \underline{E}_\theta^s]_i}{[A_{\theta\phi} * A_{\phi\theta} - A_{\phi\phi} * A_{\theta\theta}]_i} \quad (104)$$

and

$$[\underline{X}_b]_i = \frac{[A_{\phi\theta} * \underline{E}_\theta^s - A_{\theta\theta} * \underline{E}_\phi^s]_i}{[A_{\theta\phi} * A_{\phi\theta} - A_{\phi\phi} * A_{\theta\theta}]_i}. \quad (105)$$

Once  $\underline{X}_a$  or  $\underline{X}_b$  is known, Equation (92) or (93) can be used to solve for the vectors  $a$  or  $b$ . The expansion coefficients can easily be determined using Equation (53) or (65).

This procedure was applied to the resistivity functions of the previous section for sheets of dimensions  $1\lambda \times 1\lambda$  and  $5\lambda \times 5\lambda$ . Method (II) was used for convenience and the results

are, for all practical purposes identical with the original resistivity. Figures 18 and 19 compare the original and synthesized resistivity profiles (linear taper) for the  $1\lambda \times 1\lambda$  sheet and Figures 20 and 21 for the  $5\lambda \times 5\lambda$  and constant resistivity. In both cases 144 points have been used. For all the cases it was assumed that  $E_\theta^i = E_\phi^i = 1$ .

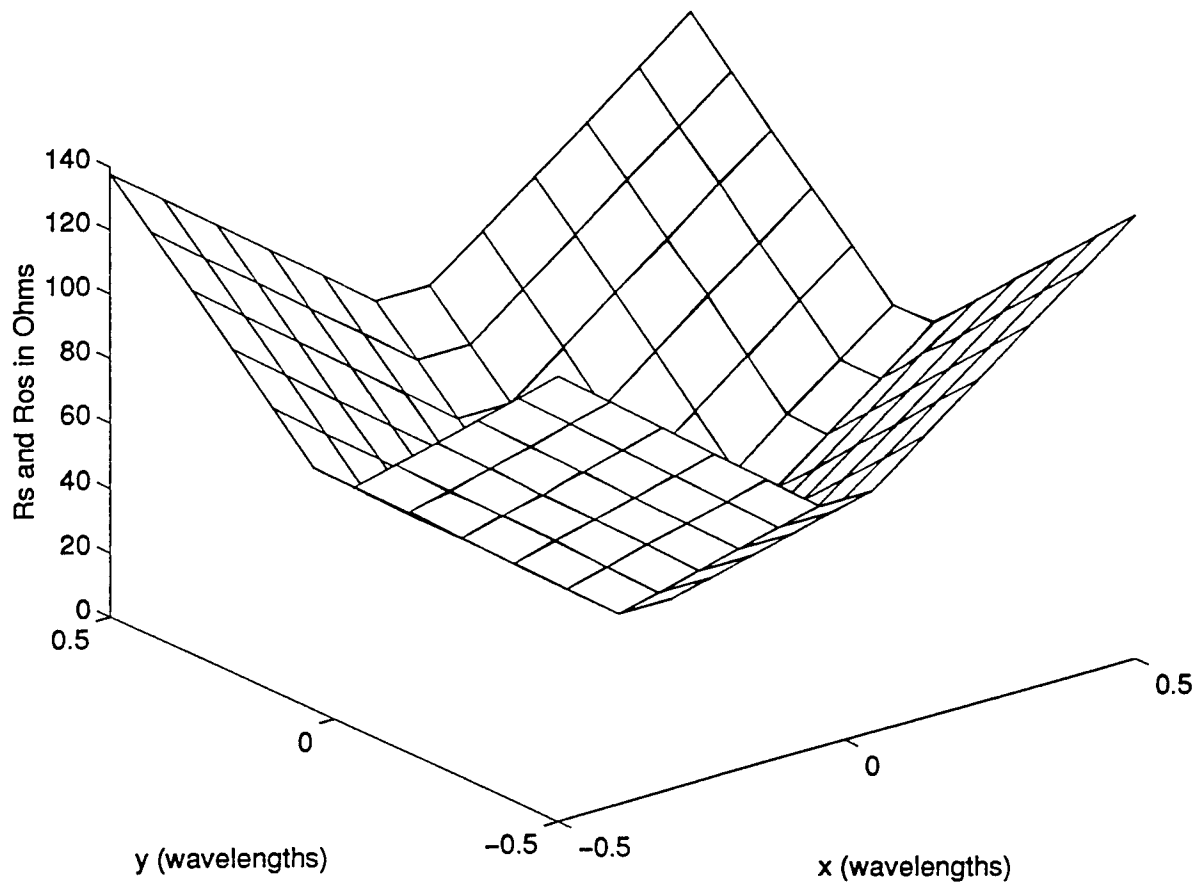


**Figure 18:** Synthesized and original resistivity distribution for arbitrary polarization. For this case,  $L_x=L_y=\lambda$ ,  $M=N=12$ ,  $N_u=N_v=12$ .

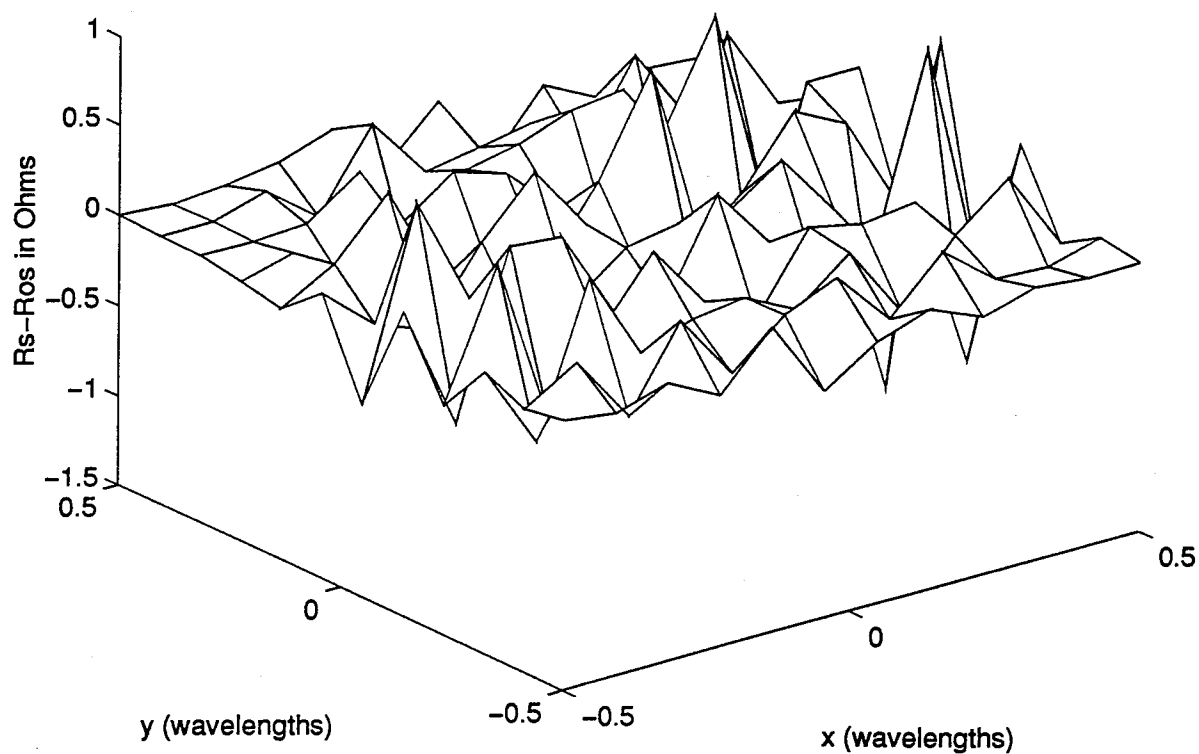


**Figure 19:** Difference in the reconstructed and the original distributions. The relative error is less than 1%.

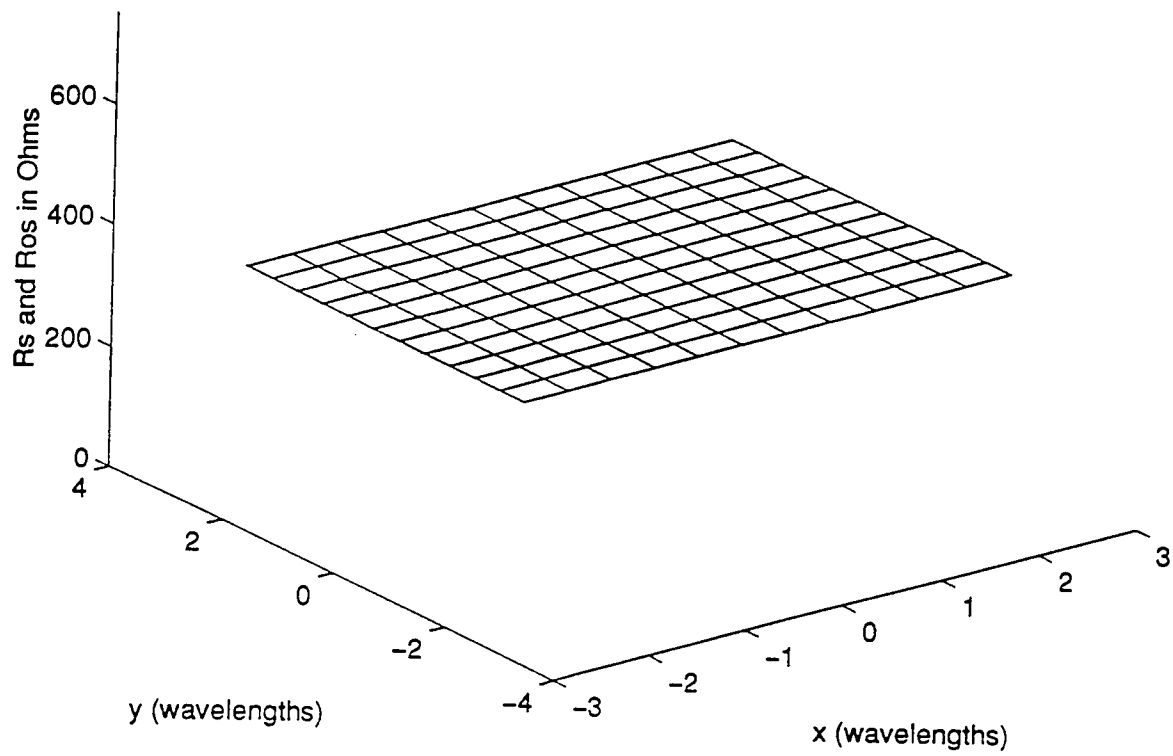


**Figure 20:** Original and synthesized resistivities for arbitrary polarization. For this case  $L_x=L_y=5\lambda$ ,  $M=N=12$ ,  $N_u=N_v=12$ ,  $E_\theta = E_\phi = 1$ .

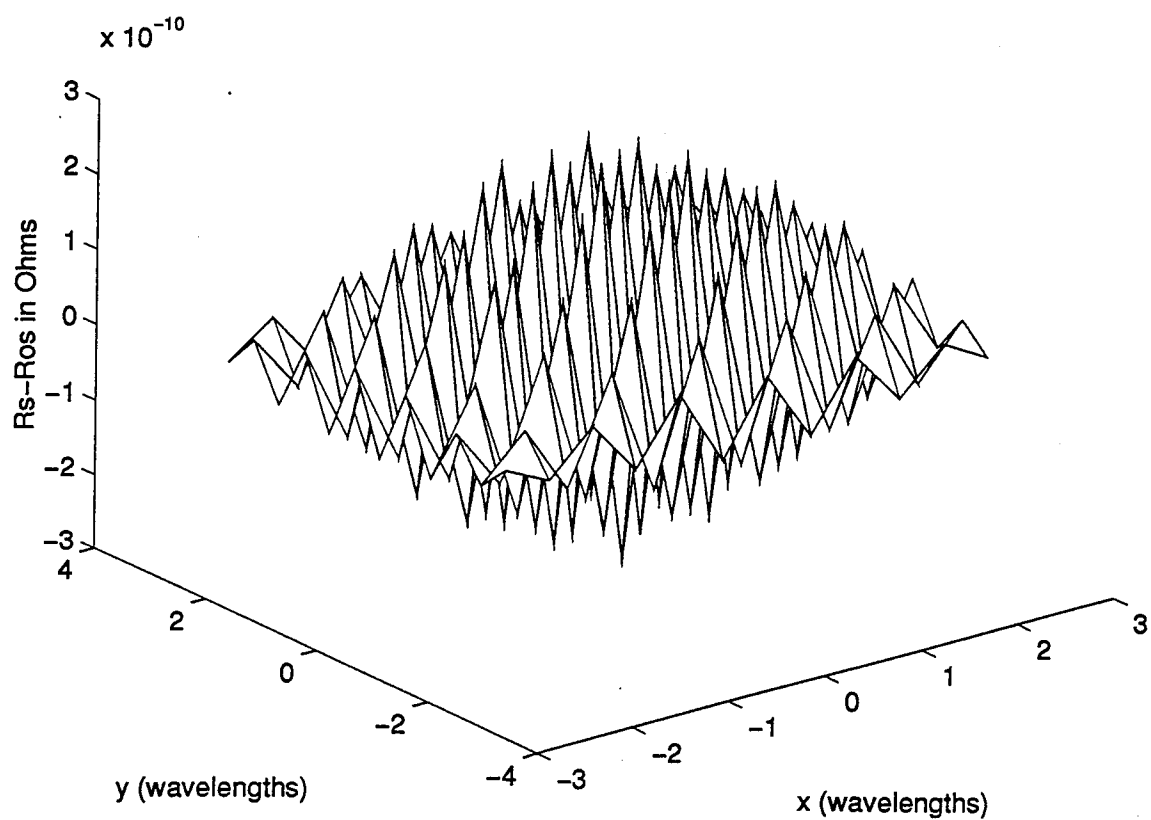


**Figure 21:** Difference in the reconstructed and the original resistivity distributions shown in Figure 20.

### C. MONOSTATIC CASE

The synthesis procedure can be applied to the monostatic case using Equation (97) or (98) for the scattered field. Alternatively, Equation (86) of the RCS can be used, which is the same for both polarizations.

Methods (I) and (II) have been investigated for two resistive sheets of sizes  $1\lambda \times 1\lambda$  and  $3\lambda \times 3\lambda$ , and the two resistivity profiles considered previously; namely a constant of  $377\Omega$ , and a linear taper given by Equation (102). The two methods give identical results.

Figure 22 compares the corresponding data for the  $1\lambda \times 1\lambda$  sheet with constant resistivity. In Figure 23 the difference between the synthesized and original distributions is plotted for a linear taper profile on a  $4\lambda \times 4\lambda$  sheet.

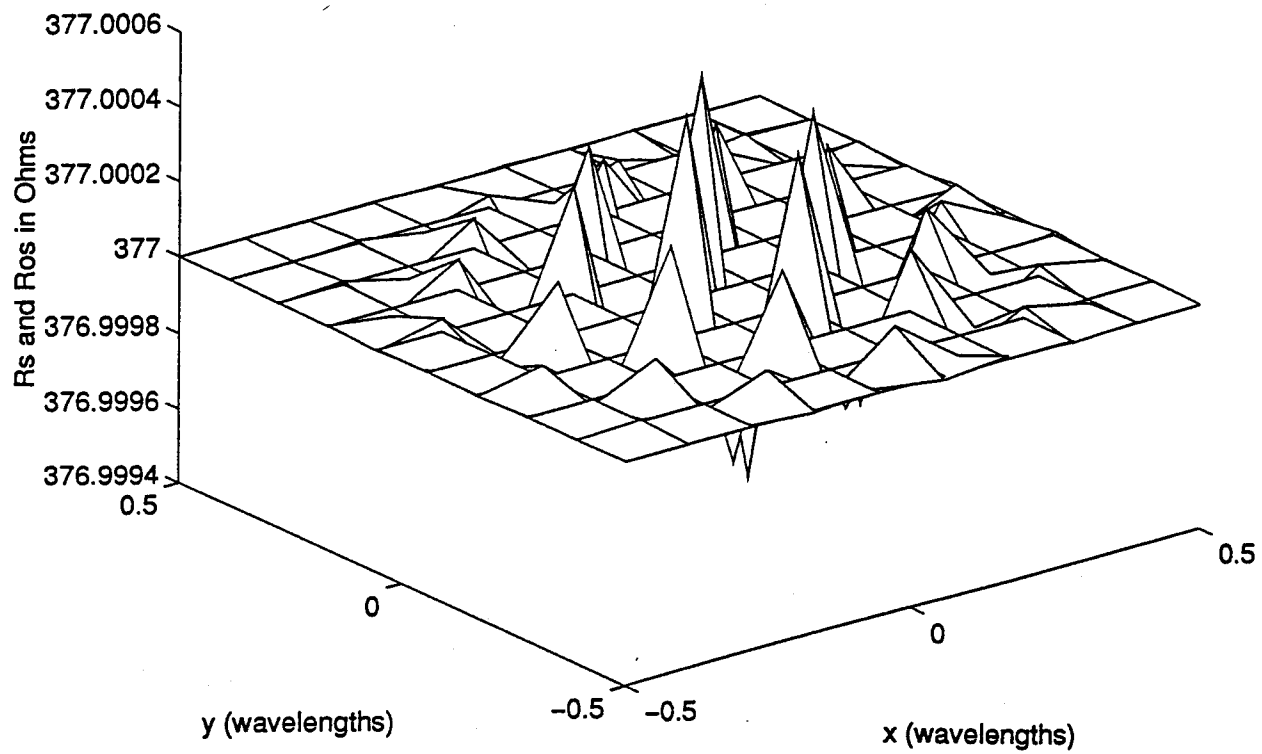


**Figure 22:** Original and synthesized resistivities for the monostatic case. On this case,  $L_x=L_y=\lambda$ ,  $M=N=12$ ,  $N_u=N_v=12$ .

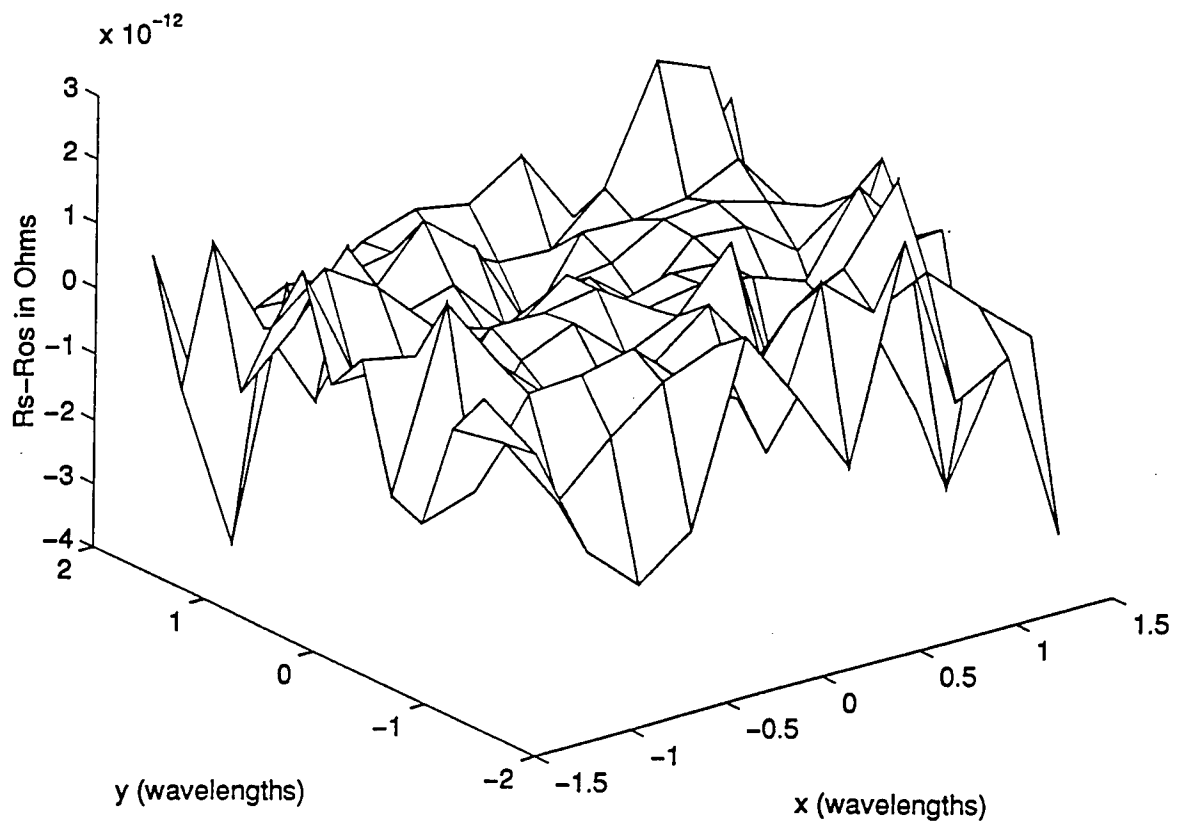


**Figure 23:** Difference in the synthesized and original linear taper resistivity for the monostatic case. For this case,  $L_x=L_y=3\lambda$ ,  $M=N=12$ ,  $N_u=N_v=12$ .

#### D. RELATION TO THE SAMPLING THEOREM

In the previous two sections it was demonstrated that the synthesis procedure works well for both methods (I) and (II) over a wide range of synthesis parameters. These calculations have verified the synthesis equations and the computational approach to solving them. So far the question of how many field points are needed to uniquely determine an unknown surface resistivity function has not been addressed.

The most critical part of the synthesis procedure is the inversion of the  $(M \times N)$  by  $(M \times N)$  matrix B. It is desirable to use the smallest number  $(M \times N)$  for computational and accuracy reasons. To find the minimum  $(M \times N)$ , a technique is borrowed from signal analysis. The scattered field is computed using a sufficiently large number of patches. The FFT is then performed on this array of field values. The result can be translated into the minimum number of patches required to accurately represent the field. This is based on the fact that plotting a field pattern (function) is basically sampling its distribution adequately. The interval between the sampled field points at which the field is computed is the sampling interval and the reciprocal of this is the sampling frequency. Dividing the u and v region into  $N_u$  and  $N_v$  segments respectively, the corresponding sampling intervals are  $2/N_u$  and  $2/N_v$ .

Nyquist's theorem [Ref. 6] requires that at least twice the maximum 'frequency component' should be used as the smallest sampling rate. Utilizing the fact that the FFT is symmetric with respect to the half of the sampling frequency used, i.e., symmetric to the  $N_u/4$  and  $N_v/4$  point, a plot of the two-dimensional FFT vs the number of segments  $N_u$  and  $N_v$  can be obtained. For simplicity an equal number of points have been used ( $N_u=N_v$ ) and the FFT is performed on the rows and the columns of the matrix of the field values to identify the

spatial frequencies in  $u$  and  $v$ . Figure 24 shows the FFT performed on the columns for the field depicted in Figure 12 using methods (I) and (II). As expected, the frequency content is the same in both cases.

In Figure 25 the spatial frequency content of the field in Figure 6 is shown. One can conclude that  $N_u$  and  $N_v$  greater than 4 is sufficient. In Figure 26 the field in the  $\phi=0$  plane is shown. The dotted line represents the field using only 16 points ( $M=N=4$ ) and the solid line the field when  $M=N=64$ .

However for the  $5\lambda \times 5\lambda$  sheet with the field shown in Figure 12 and the frequency content shown in Figure 27, 6 segments per direction should be sufficient. In Figures 28 and 29, the corresponding field plots in the  $\phi=0$  plane show the convergence.

Figure 30 shows the monostatic RCS of a  $\lambda \times \lambda$  resistive sheet. The spatial frequency content of the field is shown in Figure 31, and it reveals that 4 segments are sufficient. The corresponding field plots in Figure 32 and 33 illustrate the convergence. The same process is applied to the  $3\lambda \times 3\lambda$  plate. The frequency content is shown in Figure 34 and the corresponding convergence is shown in Figures 35 and 36.

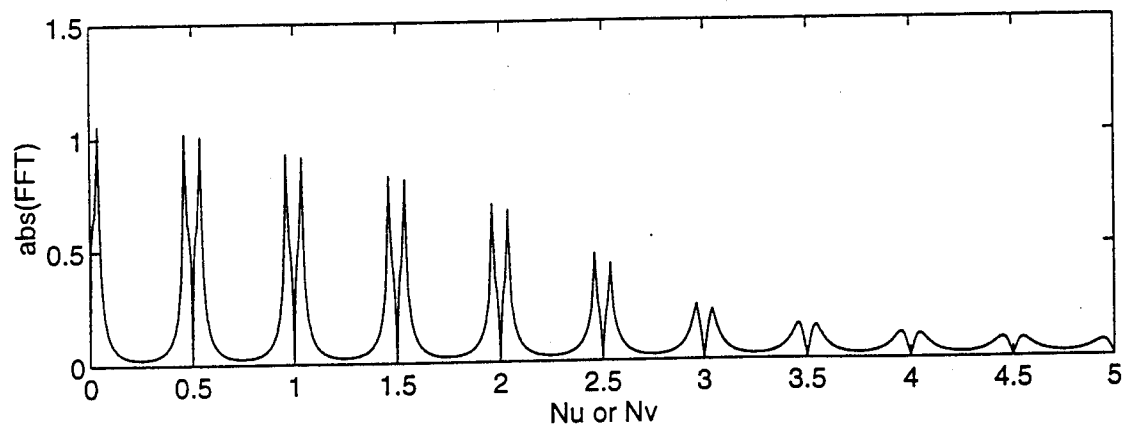
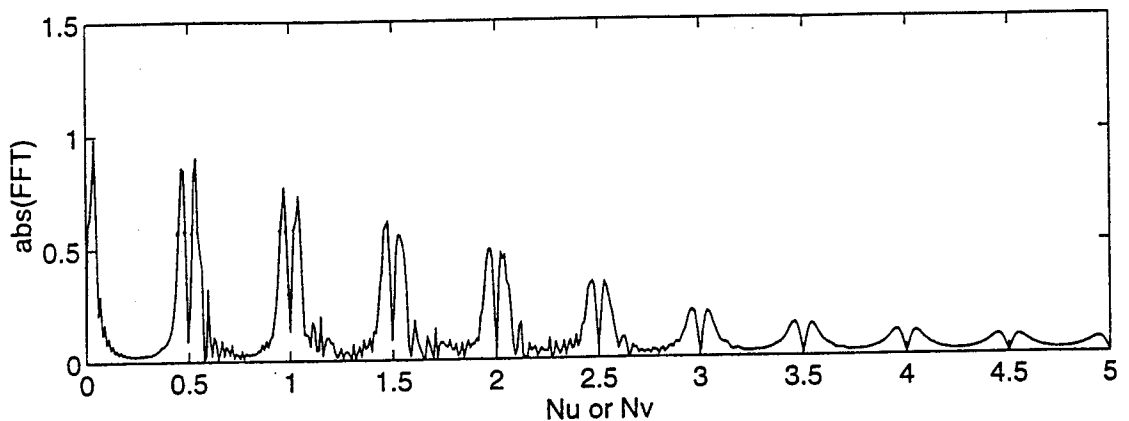


**Figure 24:** Frequency content in  $u$  direction of the bistatic scattered field shown in Figure 12 using methods (I) and (II).

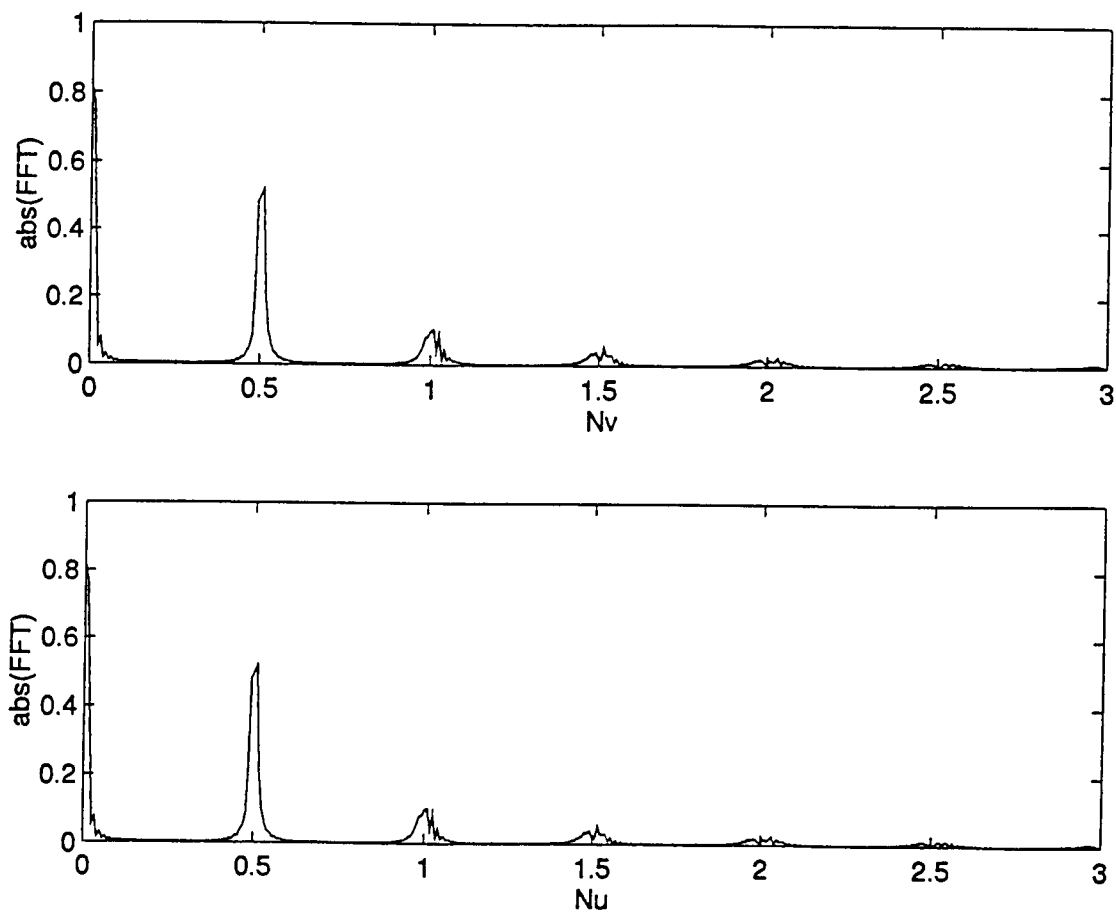


**Figure 25:** FFT of the scattered field shown in Figure 6.

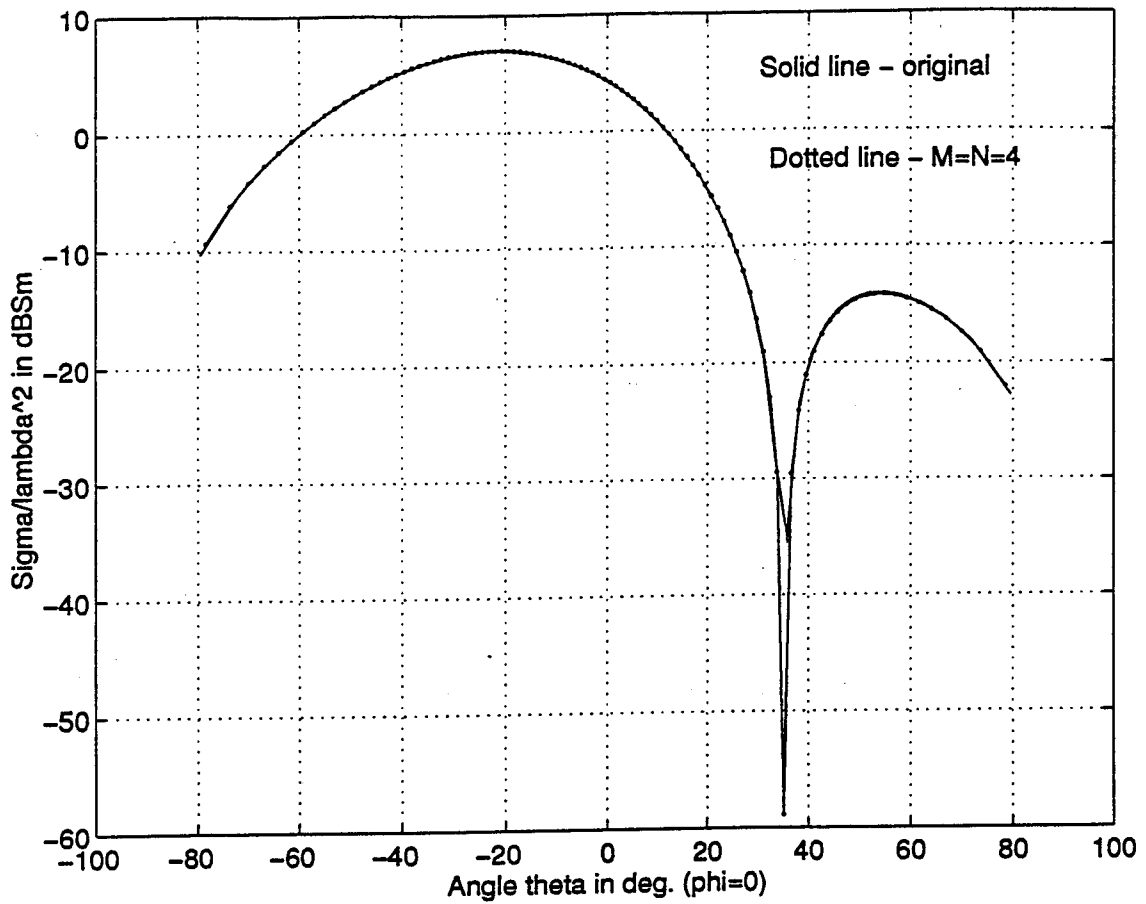


**Figure 26:** Bistatic scattered RCS in the  $\phi=0$  plane corresponds to Figure 6. The dotted line represent the RCS using the synthesized resistivity and  $M=N=4$ .

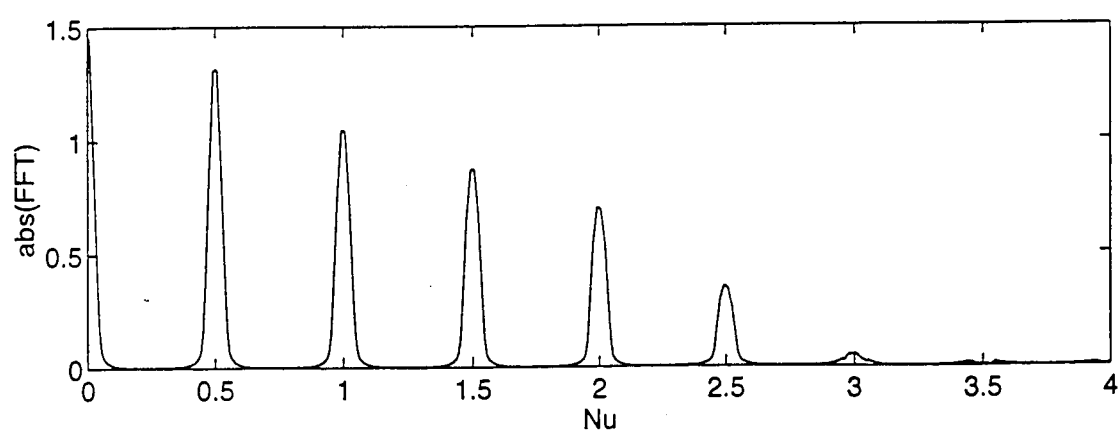
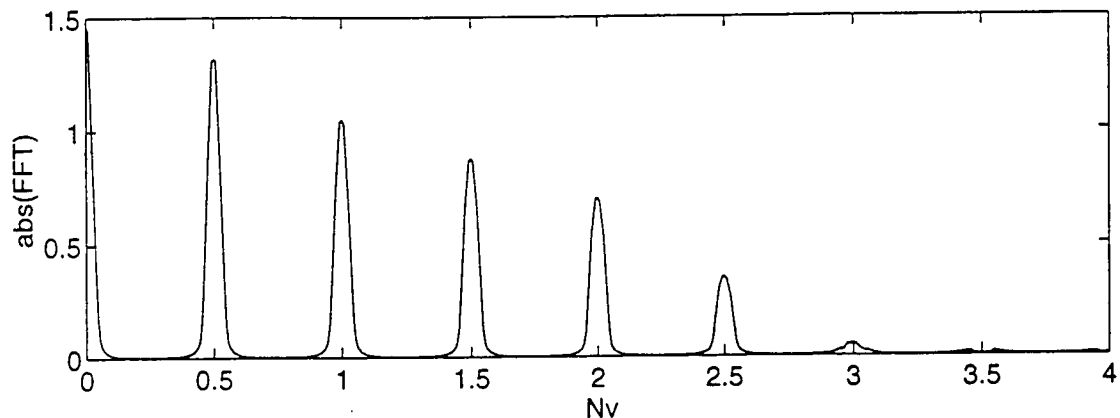


**Figure 27:** FFT in  $u$  and  $v$  directions of the bistatic scattered field in Figure 12.

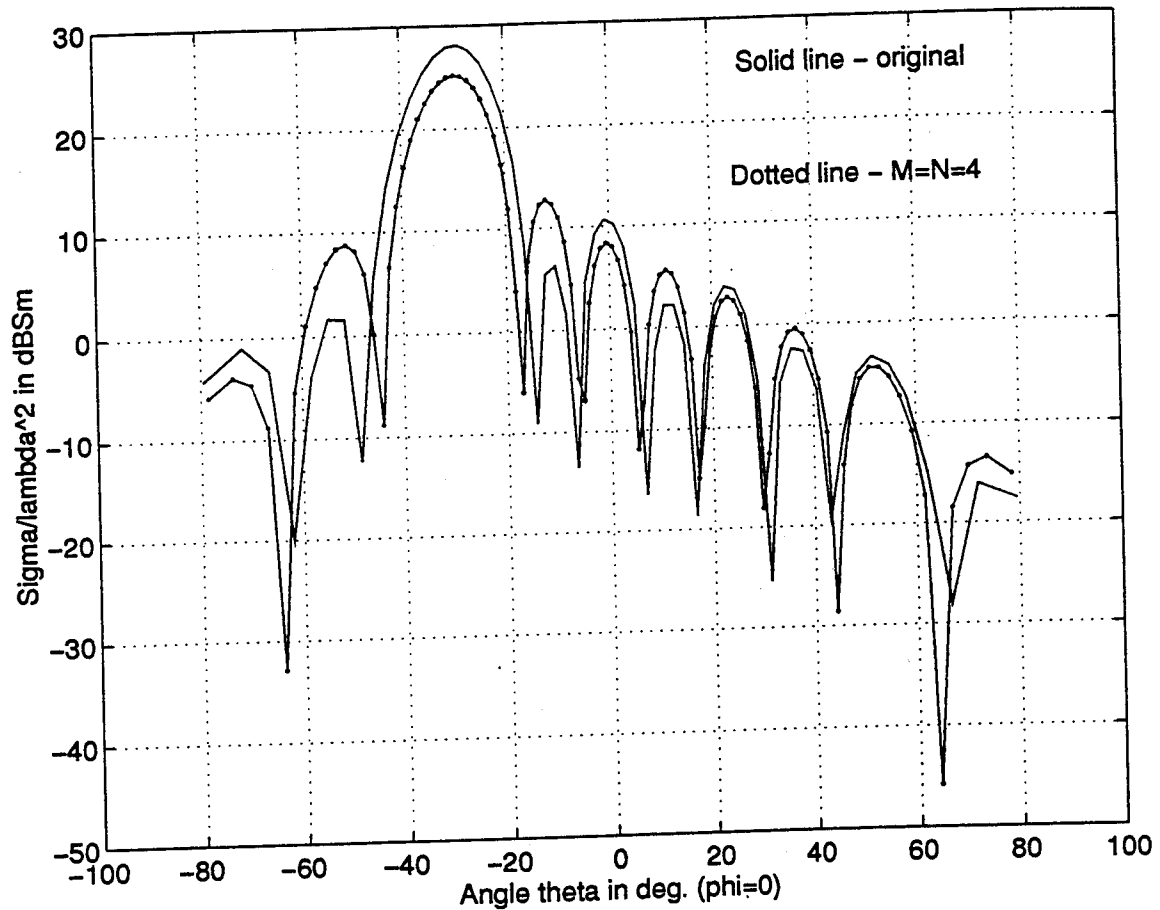


**Figure 28:** A cut on the u axis corresponding to Figure 12. The field (dotted) due to the reconstructed resistivity is within a couple of dB of the original.

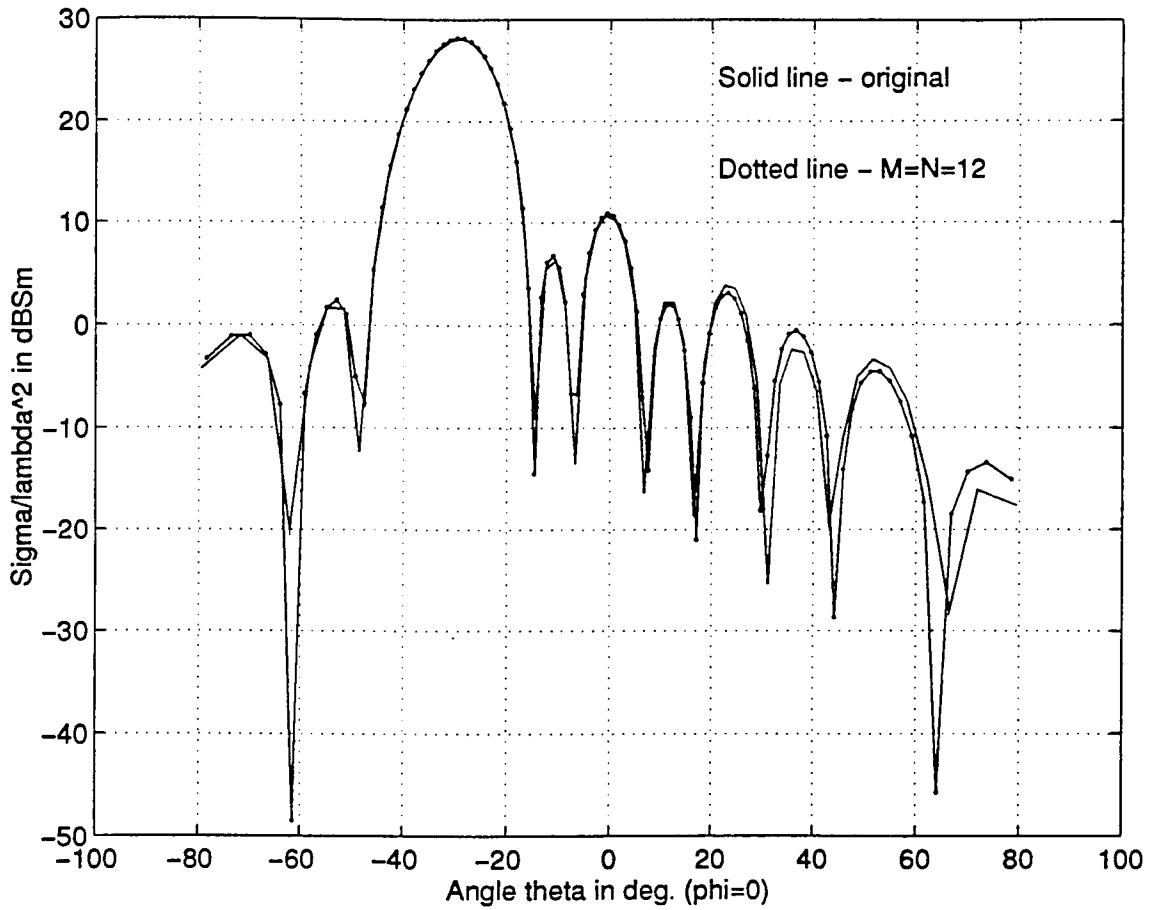


**Figure 29:** A cut on the  $u$  axis corresponding to Figure 12. Comparison of original and synthesized patterns for  $M=N=12$ .

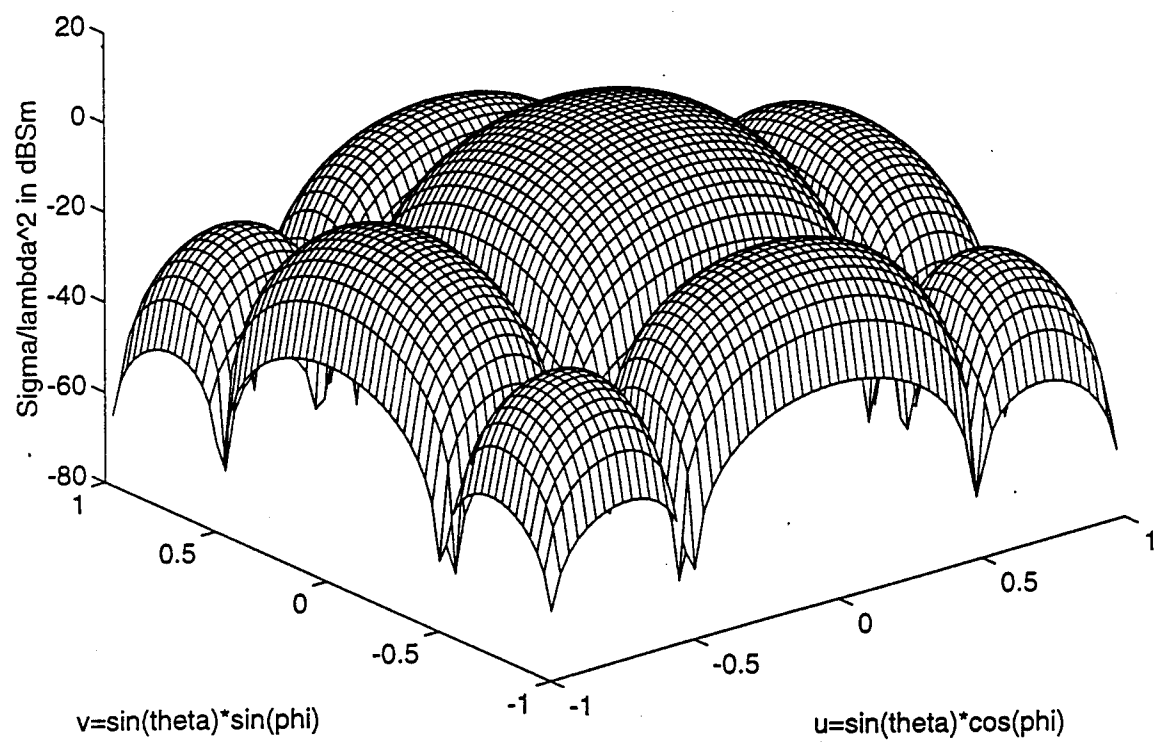


**Figure 30:** Monostatic RCS from a one wavelength square resistive sheet.  $R_s$  is given by Equation (102).

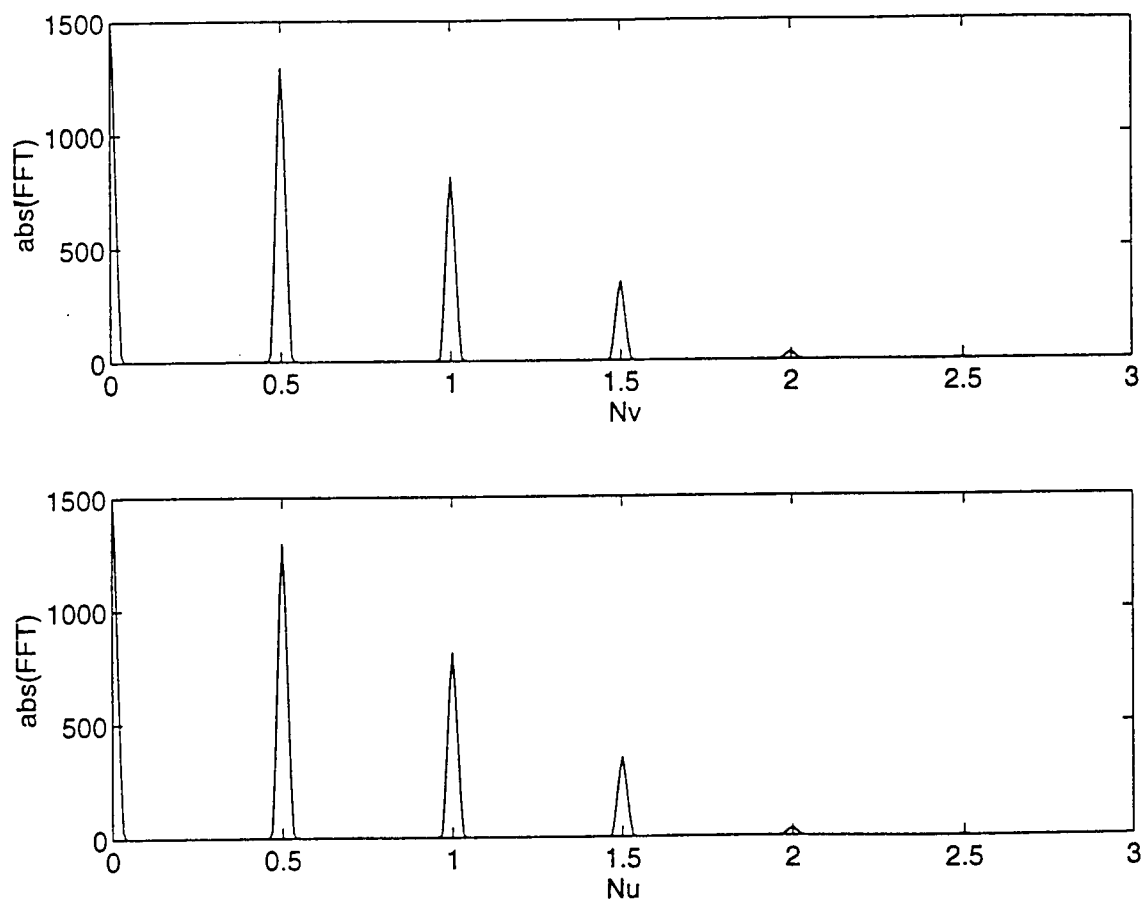


**Figure 31:** FFT of the monostatic scattered field in Figure 30.

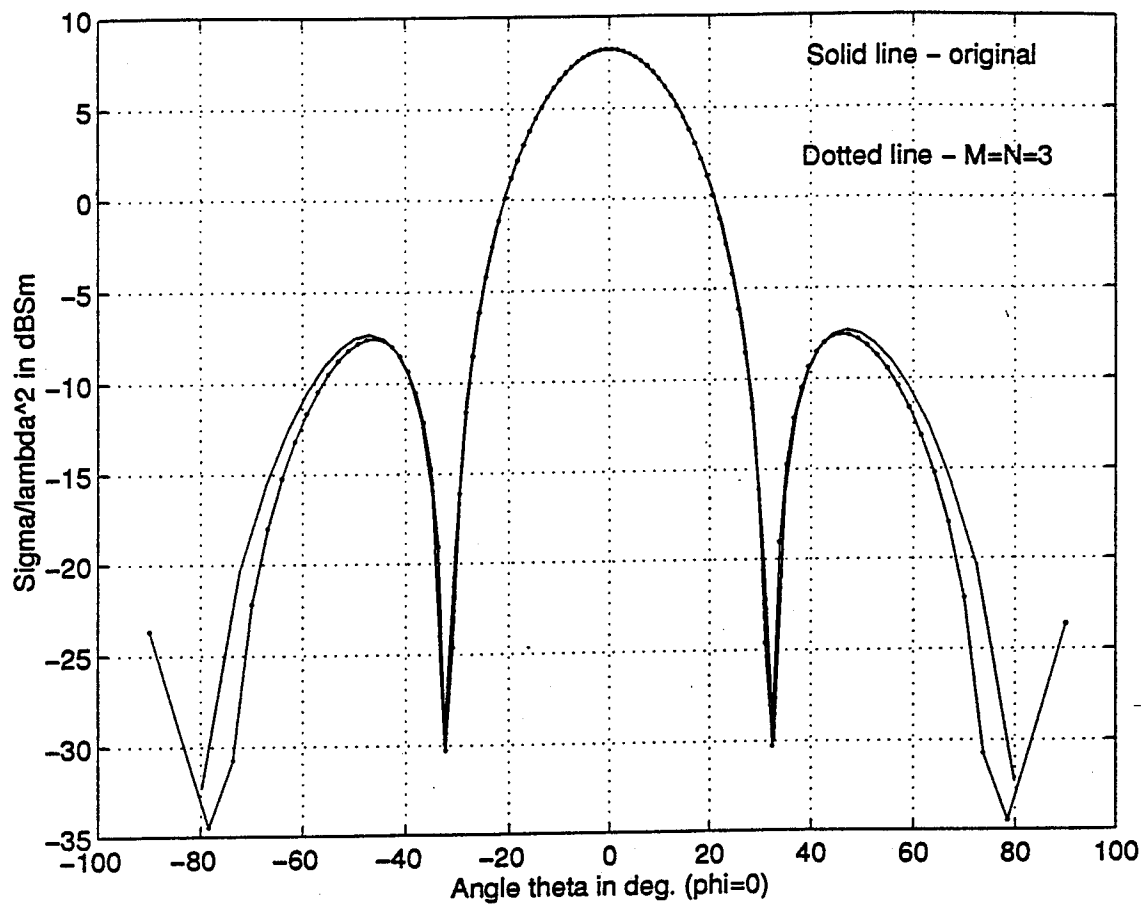


**Figure 32:** The monostatic RCS due the reconstructed resistivity with 9 patches compared to the original.

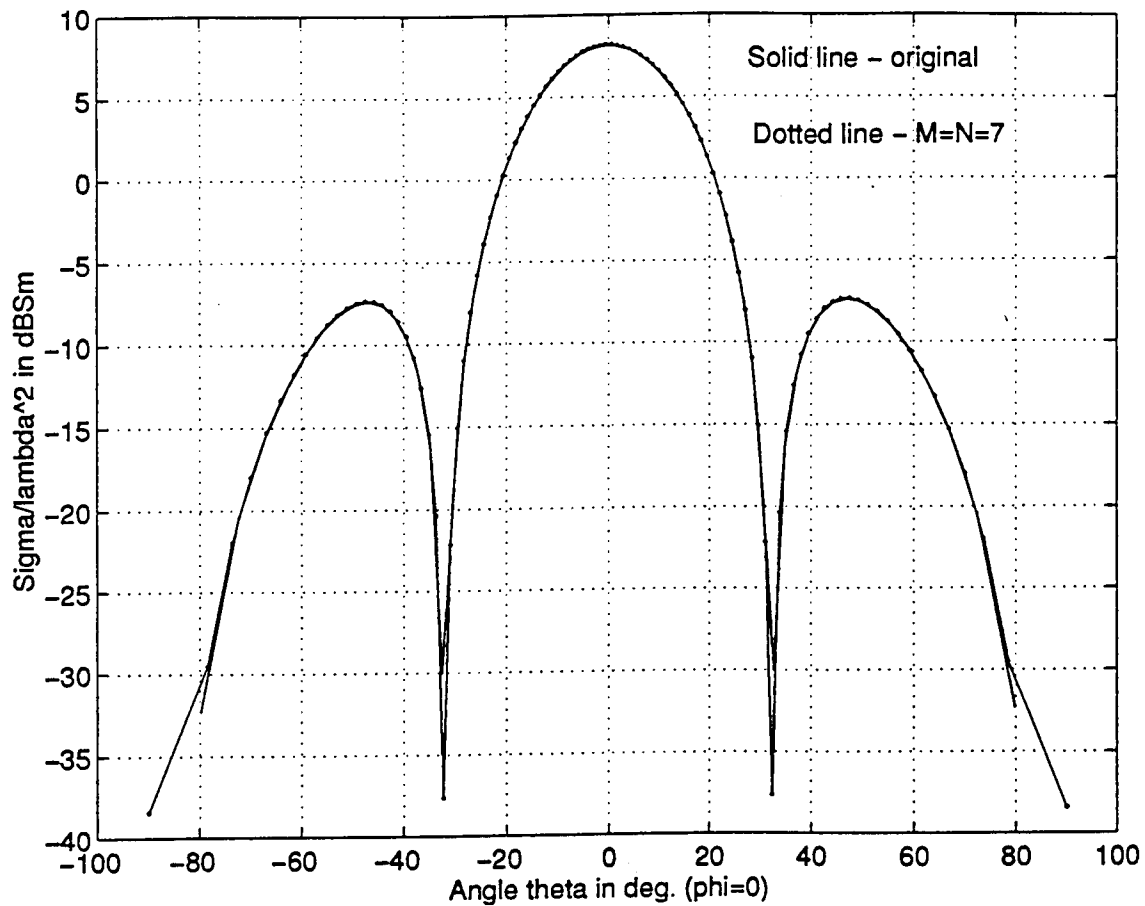


**Figure 33:** Using  $M=N=4$ , the monostatic RCS due to the reconstructed resistivity profile is converged.

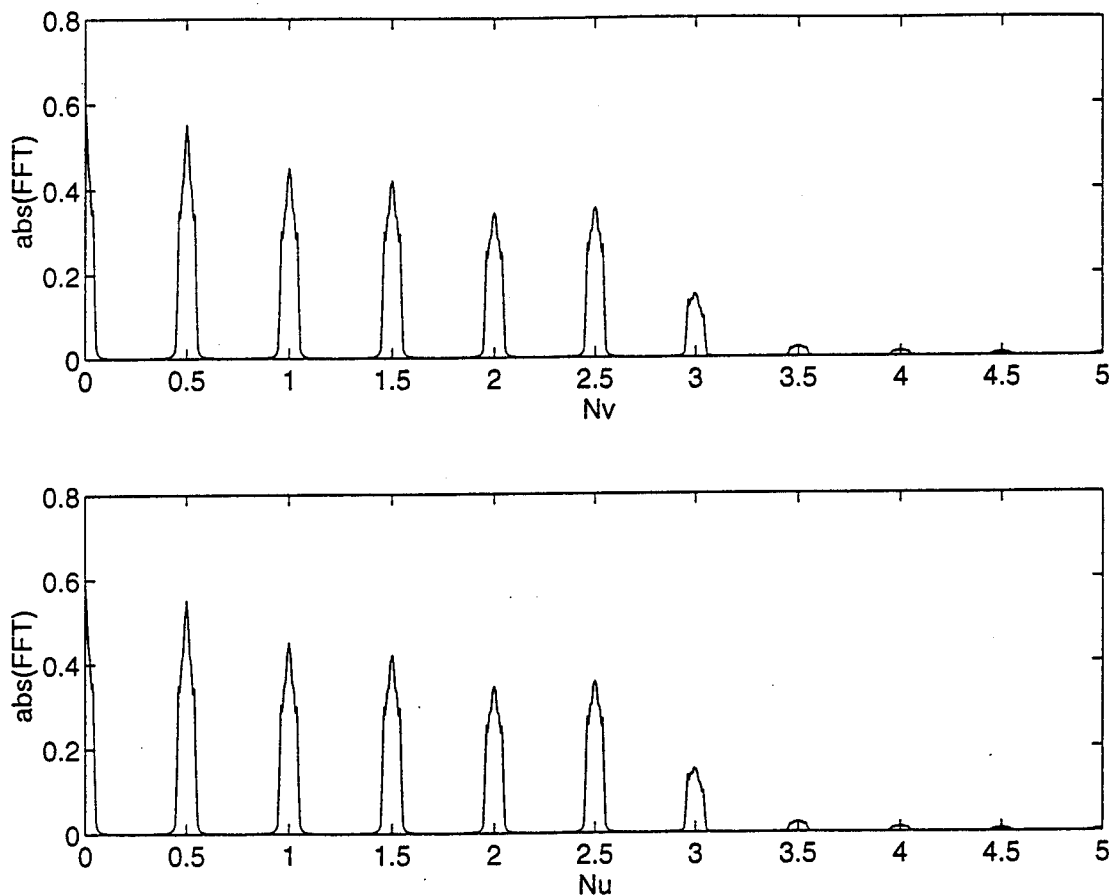


**Figure 34:** FFT of the monostatic scattered field from a resistive sheet with  $L_x = L_y = 3 \lambda$ .

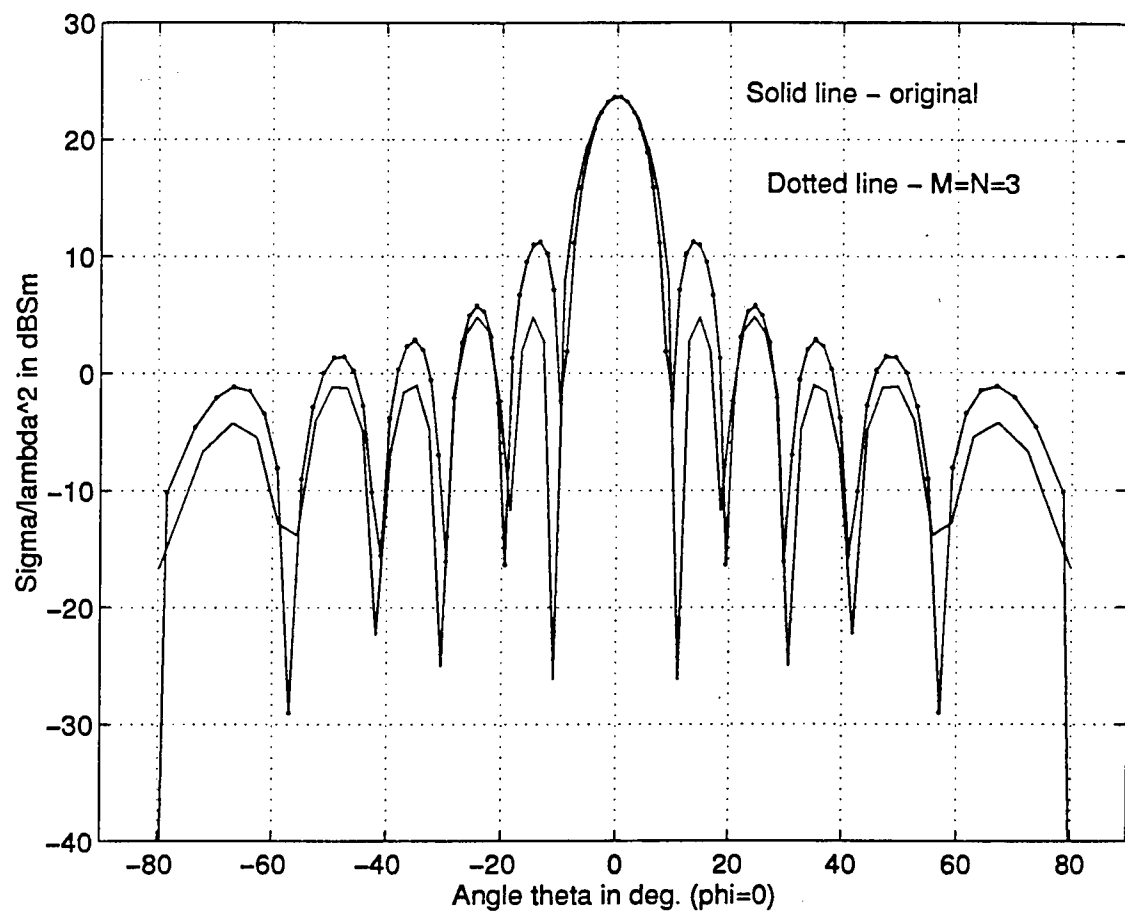


**Figure 35:** The monostatic scattered field due to the reconstructed resistivity (dotted) compared to the original for  $M=N=4$ .

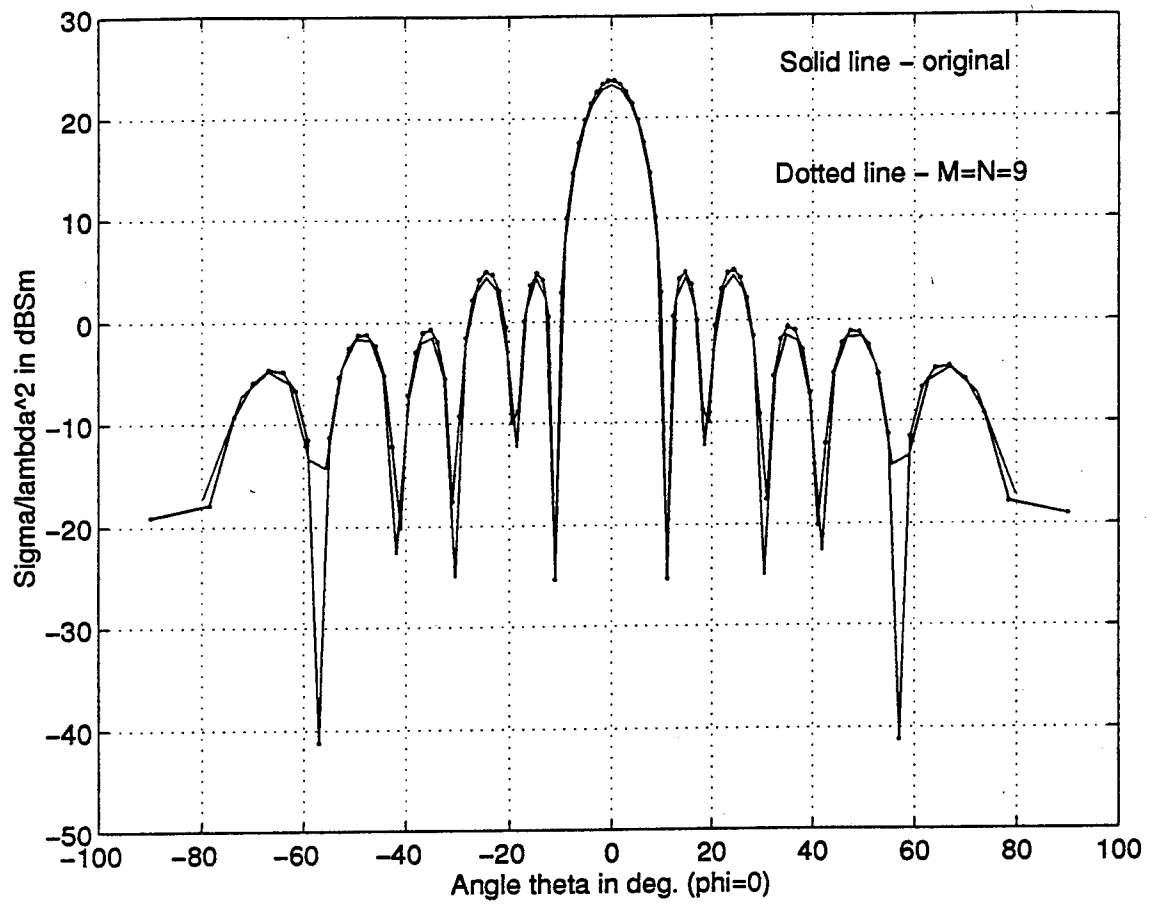


**Figure 36:** Using  $M=N=12$  the monostatic scattered field due to the reconstructed resistivity is converged. For this case  $L_x=L_y=3\lambda$ .

## E. SUMMARY

In this chapter the synthesis procedure was computer simulated and the corresponding data were presented. Two methods were investigated for choosing observation points for generating synthesized distributions. In method (I) points inside of the visible region were used. This gives good results, but it was shown to be very restrictive because the number of observation points in the visible region must match the number of subdomains on the plate. By allowing complex angles it is possible to use observation points in the entire region bounded by  $-1 \leq u, v \leq 1$  (method (II)). This is much more flexible and still gives good results.

Using Fourier analysis and the sampling theorem it was possible to identify the minimum number of patches that can be used in the synthesis procedure. In general the larger the sheet the more points are necessary, and consequently the computing time increases significantly.

To illustrate the procedure two resistive sheets were considered,  $1\lambda \times 1\lambda$  and  $5\lambda \times 5\lambda$  for the bistatic case and  $1\lambda \times 1\lambda$  and  $3\lambda \times 3\lambda$  for the monostatic case. The method was tested first from the computational point of view. For the resistivity distributions considered (constant and linear taper) it was found that patch dimensions of approximately  $0.5\lambda$  and  $0.25\lambda$  were sufficient in the bistatic and monostatic cases, respectively, to obtain good agreement with the original scattered field.

## V. CONCLUSIONS

A method of RCS synthesis for planar resistive sheets has been presented. The synthesis equations were developed assuming that the resistive sheet boundary conditions hold at all points on the surface. Therefore the equations implicitly neglect the effect of the edges on the current.

The equations were verified by first calculating the RCS of the resistive sheet for a known resistivity function and then using these values for back solution to obtain a synthesized surface resistivity. In principle the two resistivity functions should be identical, but because of numerical roundoff the agreement is not exact. However, the results for a wide range of synthesis parameters were in very close agreement with the original resistivity distributions.

It was also shown that a Fourier decomposition of the scattering pattern yields guidelines for choosing the subdomain size, or equivalently, the number of far field observation points. It was found that a subdomain size of about  $0.5\lambda$  for bistatic RCS and  $0.25\lambda$  for monostatic RCS give converged results. By convergence is meant that RCS for the synthesized distribution is essentially the same as the RCS for the original scattered distribution.

It is important to note that the synthesis is based on a particular assumption with regard to the form of the current. The resistive sheet boundary condition is equivalent to the physical optics approximation in the sense that the current in the vicinity of the edge is not disturbed by the presence of the edge. The current is only a function of the incident field and the surface resistivity (see Equation (4)). Thus using the synthesized resistivity distribution in a method of moments code could yield a RCS substantially different from that based on the assumed current if surface waves exist. Examples are shown in Figures 37 and 38. In these cases the surface waves

are not as strong as they would be for a surface with more highly conducting edges, and therefore the agreement between the two curves is relatively close. This problem is overcome if the current is treated as an unknown along with the resistivity. This approach allows a rigorous solution of the problem and is recommended that future work is directed along these lines.

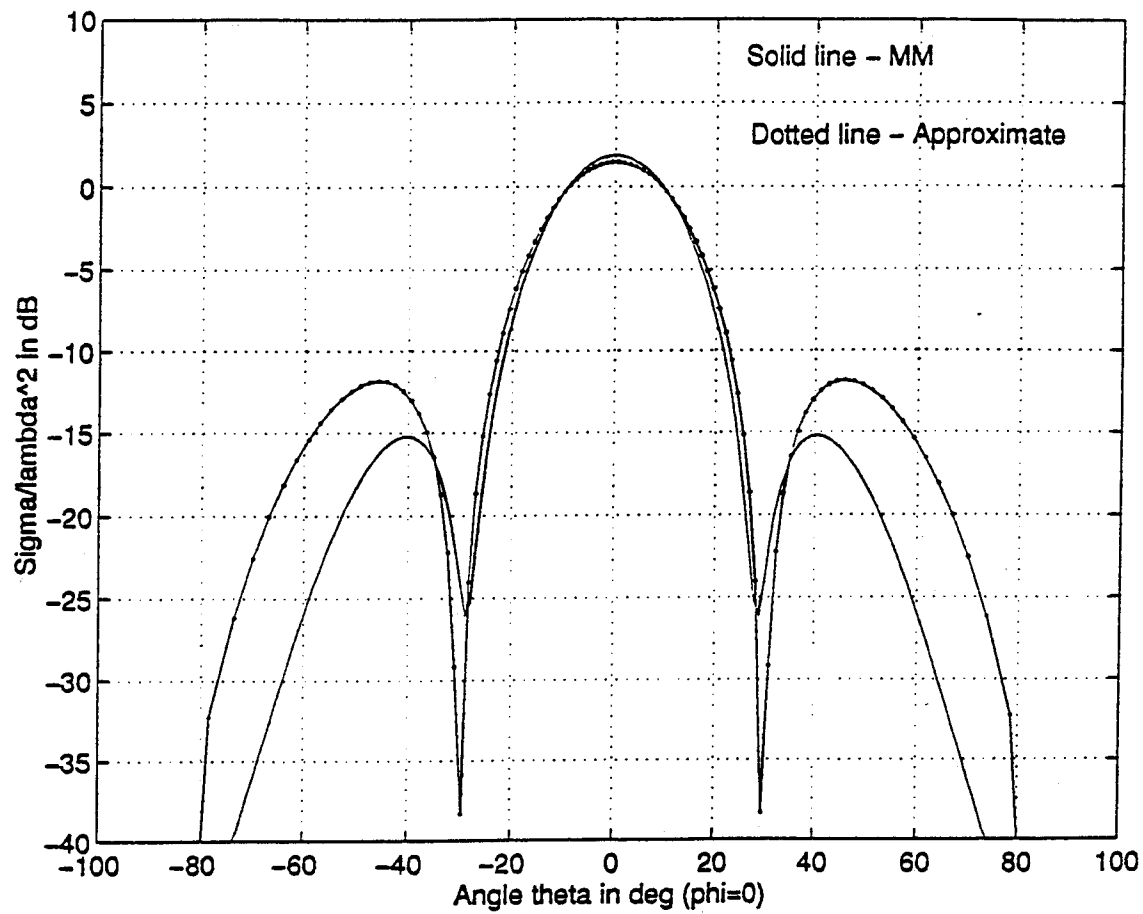


**Figure 37:** Comparison of the monostatic RCS using MM and the approximate method. For this case,  $L_x=L_y=\lambda$ ,  $M=N=12$ ,  $N_u=N_v=12$ .  $R_s = 377\Omega$ .

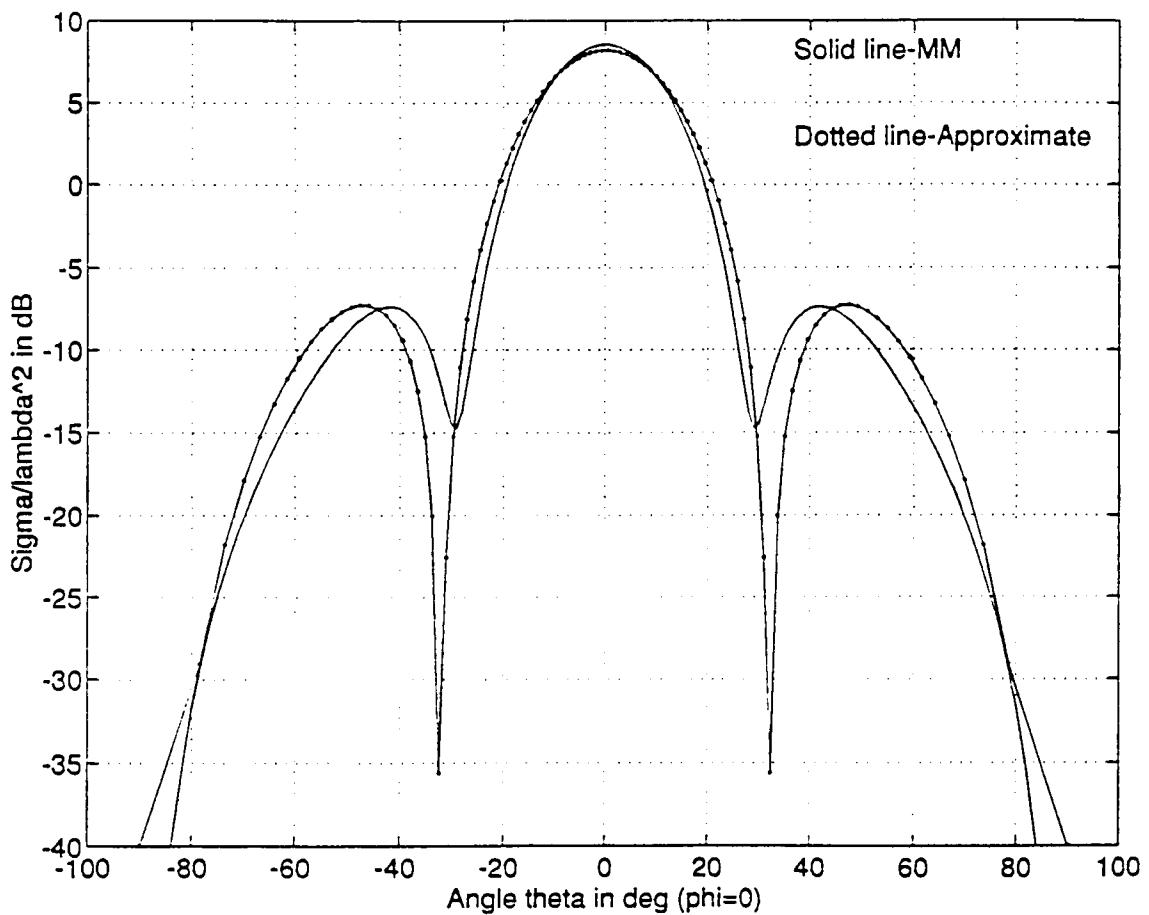


**Figure 38:** Comparison of the monostatic RCS using MM and the approximate method.  $L_x=L_y=\lambda$ ,  $M=N=12$ ,  $N_u=N_v=12$ .  $R_s$  is given by Equation (102).

## APPENDIX. COMPUTER CODES

This appendix contains the codes developed to computer simulate the synthesis equations. Code **field.m** calculates the scattered field or RCS for each case (monostatic, bistatic, method (I), method (II)), given the size of the resistive sheet and the surface resistivity. Code **synth.m** uses the field values calculated from **field.m**, to synthesize the surface resistivity. Code **synth1d.m** uses the surface resistivity values calculated by **synth.m** to plot the RCS in the  $\phi=0$  plane. Code **fanalys1.m** performs the FFT analysis for methods (I) and (II), and code **fanalys2.m** performs the FFT analysis in the u and v direction of the scattered field. Function **coord.m** is used in the first two codes to find the coordinated of the patches given the size of the sheet and the number of patches. Finally, program **fit.m** finds the closest number of points closest to an input value that fit in the unit circle, and is used in method (I).

```

%
% Program field.m

%
% This program calculates for a rectangular sheet:

%
% (i) Bistatic case: ( $\sigma_{\theta\theta}$ , or
%  $\sigma_{\phi\phi}/\lambda^2$ )
%
% or the
%
% scattered field for the general case
%
% of the
%
% incident field, given the values
%
%  $E_{th_i}$  and
%
%  $E_{phi_i}$  and assuming  $Co=1$ .

%
% (ii) Monostatic case:  $\sigma/\lambda^2$ 

%
% The plate can be PEC or resistive. Plots of the
% resistance,
%
% as well as, 3-D plots of the field are shown.
%
% Works in the direction cosine space.

%
% Date: 10 Nov 1994
%
% By: Nick Faros.

clear

%%%%% INPUT PARAMETERS %%%%

choice1=input('Enter 1 for bistatic or 0 for monostatic: ');

```

```

choice2=input('Enter 1 for method (II) or 0 for method (I):
');

a1=input('Enter size in -x (multiples of wavelength): ');
b1=input('Enter size in -y (multiples of wavelength): ');

% Assume wavelength l=1
l=1;
k=2*pi/l;           % wavenumber
a=a1*l;             % dimension in x (in meters)
b=b1*l;             % dimension in y (in meters)

Nx=input('Enter # of patches in x (N): ');
Ny=input('Enter # of patches in y (M): ');

dx=a/Nx;            dy=b/Ny;
xx=-a/2:a/(Nx-1):a/2; yy=-b/2:b/(Ny-1):b/2;

% xx,yy are the dimension of the plate in meters

R=input('Resistance:0=PEC, 1=constant, 2=linear taper,
3=ramp:');
if R==1
    c1=input('Enter constant value: ');
end

tic

%%%%%%%%%%%%%%%
%%% FIND COORDINATES OF THE PATCHES %%%%
[xo,yo]=coord(a,b,Nx,Ny); % Call function coord.m

```

```

x1=reshape(xo,1,Nx*Ny);
y1=reshape(yo,1,Nx*Ny);

%%%%%%%%%      FIND PATTERN OF THE INPUT RESISTANCE      %%%%%%%

% Some cases

if R==0
    r=zeros(Ny,Nx);          % Zero everywhere
elseif R==1
    r=c1*ones(Ny,Nx);      % Constant
elseif R==2
    r=abs(xo)+abs(yo);    % linear taper in both dimensions
    r=150*r;
elseif R==3
    r=zeros(Ny,Nx);
    for l=1:Nx
        r(:,l)=100*l*ones(Ny,1);  % ramp
    end
end
r1=reshape(r,1,Nx*Ny);

%%%%%%%%%%%%%%

% Next find coordinates of the center of the patches in
% direction cosine space. If method (I) is used, run fit.m
% first, to find nx, ny. If method (II) is used nx=Nx and
% ny=Ny;

if choice2==1      % Method (II)

```

```

nx=Nx;
ny=Ny;

elseif choice2==0 % Method (I)
    nx=4      % Nu
    ny=5      % Nv
end

[u,v]=coord(2,2,nx,ny);
u1=reshape(u,1,nx*ny);
v1=reshape(v,1,nx*ny);

%%%%%%%%%%%%%
sintheta=sqrt(u1.^2 +v1.^2);
I=find(sintheta>1);
phi=atan2(v1,u1);
costheta=sqrt(1-sintheta.^2);
if choice2==0 % Method (I)
phi(I)=[]; costheta(I)=[]; sintheta(I)=[];
u1(I)=[]; v1(I)=[];
end
%%%%%%%%%%%%%

%       %%%%%% BISTATIC CASE %%%%%%
if choicel==1      % Bistatic

    thid=input('Enter theta inc. in degrees: ');
    thir=thid*pi/180; % translate it into radians

    phiid=input('Enter phi inc. in degrees: ');
    phiir=phiid*pi/180;

```

```

coef1=1./(2*r1+377*cos(thir)); % bistatic
coef2=1./(2*r1*cos(thir)+377); % bistatic

% u=sin(theta)*cos(phi)
% v=sin(theta)*sin(phi)

ui=sin(thir)*cos(phiir);
vi=sin(thir)*sin(phiir);

sinc1=sin(k/2*dx*(u(1,:)+ui))./(k/2*dx*(u(1,:)+ui));
S1=find(isnan(sinc1));
sinc1(S1)=ones(size(S1));

sinc2=sin(k/2*dy*(v(:,1)+vi))./(k/2*dy*(v(:,1)+vi));
S2=find(isnan(sinc2));
sinc2(S2)=ones(size(S2));

sinc=sinc2*sinc1;
sinc=reshape(sinc,1,nx*ny);
if choice2==0
sinc(I)=[] ;
end

choice3=input('Enter 1 for sigma_theta_theta, 2 for
sigma_phi_phi, or 3 for the general scattered field: ');

if choice3==1 % Compute sigma_theta_theta

for p=1:Ny*Nx
expn=exp(j*k*(x1*(u1(p)+ui)+y1*(v1(p)+vi)));
s1(p)=(expn*conj(coef1'));

```

```

end

%E=dx*dy*cos(thir)*costheta.*sinc.*cos(phi-phiir).*s1;
E=dx*dy*cos(thir)*costheta.*sinc.*cos(phiir).*s1;

RCS1=((377*2*pi*E).^2)./pi;

RCS=10*log10(abs(RCS1));
RCS=reshape(RCS,Ny,Nx);

elseif choice3==2 % Compute sigma_phi_phi

for p=1:Ny*Nx
    expn=exp(j*k*(x1*(u1(p)+ui)+y1*(v1(p)+vi)));
    s2(p)=(expn*conj(coef2'));
end

E=dx*dy*cos(thir)*sinc.*cos(phi-phiir).*s2;
RCS1=(377*2*pi*E).^2./pi;

RCS=10*log10(abs(RCS1));
RCS=reshape(RCS,Ny,Nx);

elseif choice3==3 % Compute field

Eth_i =input('Enter magnitude Eth_i: ');
Ephi_i =input('Enter magnitude Ephi_i: ');

for p=1:Ny*Nx
    expn=exp(j*k*(x1*(u1(p)+ui)+y1*(v1(p)+vi)));
    s1(p)=(expn*conj(coef1'));
end

```

```

for p=1:Ny*Nx
    expn=exp(j*k*(x1*(u1(p)+ui)+y1*(v1(p)+vi)));
    s2(p)=(expn*conj(coef2'));
end

E_th=dx*dy*cos(thir)*costheta.*sinc.* (Eth_i*cos(phi-phiir).*s1+Ephi_i*sin(phi-phiir).*s2);

E_phi=-dx*dy*cos(thir)*sinc.* (Eth_i*sin(phi-phiir).*s1-Ephi_i*cos(phi-phiir).*s2);

E=sqrt((abs(E_th)).^2+(abs(E_phi)).^2);
E1=reshape(E,Ny,Nx);

end

if choice3==3
    save fnb a b E_th E_phi Eth_i Ephi_i r ui vi thir
    phiir u1 v1 x1 y1 xx yy choice3 choice2 % Use in synth.m
else
    save fnb a b E r ui vi thir phiir u1 v1 x1 y1 xx yy
choice3 choice2 % Use in synth.m
end

```

%%%%%%%%%%%%%% MONOSTATIC CASE %%%%%%%%%%

```

elseif choice1==0

sinc1=sin(k*dx*u(1,:))/(k*dx*u(1,:));

```

```

S1=find(isnan(sinc1));
sinc1(S1)=ones(size(S1));

sinc2=sin(k*dy*v(:,1))./(k*dy*v(:,1));
S2=find(isnan(sinc2));
sinc2(S2)=ones(size(S2));

sinc=sinc2*sinc1;
sinc=reshape(sinc,1,nx*ny);

coef=1./(2*r1+377); % monostatic

for p=1:Ny*Nx
    expn=exp(2*j*k*(x1*u1(p)+y1*v1(p)));
    s(p)=(expn*conj(coef'));
end

E=dx*dy*sinc.*s;
RCS1=(377*2*pi*E).^2/pi;
RCS=10*log10(abs(RCS1));
RCS=reshape(RCS,Ny,Nx);

if choice2==1 % Method II

    save fnm a b E u1 v1 x1 y1 r xx yy choice2 % Use it in
synth.m
elseif choice2==0 % Method (I)

    E(I)=[];
    save fnm a b E u1 v1 x1 y1 r xx yy choice2 % Use it in
synth.m

end
end

```

```

save nf E Nx Ny I    % Use in fanalys.m

time=toc

%%%%% PLOTS %%%%
if choice1==1
if choice2==1 % Method (II)
if choice3==1 | choice3==2
figure(1);mesh(xx,yy,real(r)), xlabel('Size in x')
ylabel('Size in y'), zlabel('Ohms')

figure(2)
mesh(u,v,RCS)
xlabel('u=sin(theta)*cos(phi)')
ylabel('v=sin(theta)*sin(phi)')
zlabel('Sigma/lambda^2 in dBSm')

sint=u(1,:);
th=asin(sint); th=th*180/pi;
figure(3)
plot(th,RCS(Ny/2,:)), grid
xlabel('Angle theta in deg. at phi=0 plane')
ylabel('Sigma/lambda^2 in dBSm')

RCS1=reshape(RCS1,Nx,Ny);
mesh(u,v,abs(RCS1))
end
end

elseif choice1==0
figure(1);mesh(xx,yy,real(r)), xlabel('Size in x')
ylabel('Size in y'), zlabel('Ohms')

```

```

figure(2)
mesh(u,v,RCS)
xlabel('u=sin(theta)*cos(phi)')
ylabel('v=sin(theta)*sin(phi)')
zlabel('Sigma/lambda^2 in dBSm')

sint=u(1,:);
th=asin(sint); th=th*180/pi;
figure(3)
plot(th,RCS(Ny/2,:)),grid
xlabel('Angle theta in deg. at phi=0 plane')
ylabel('Sigma/lambda^2 in dBSm')

RCS1=reshape(RCS1,Nx,Ny);
mesh(u,v,abs(RCS1))
end
end
end
save mf RCS th

```

```

%                                         Code synth.m

% This code reads from the files fn*.mat (output of
% the code field.m), RCS or field values at specific
% points, and synthesizes the surface resistivity.
% This code divides the sheet and DCS into 'big'
% patches compared to the field.m code. The number of
% patches should be chosen such that the center of
% the big patch, coincides with the center of a small.
% So, the big patch must contain an odd number of
% smaller patches.
% Note that the codes field.m and synth.m can also
% have the same number of patches.

% Works for monostatic and bistatic case.
clear

choice1=input('Enter 1 for bistatic or 0 for monostatic: ');

if choice1==1
    load fnb
elseif choice1==0
    load fnm
end

k=2*pi;
Nx=input('Enter # of patches in x (N): ');
Ny=input('Enter # of patches in y (M): ');

% Nx, Ny are the 'big' patches.
tic
Dx=a/Nx;                               Dy=b/Ny;
XX=-a/2:a/(Nx-1):a/2;                  YY=-b/2:b/(Ny-1):b/2;

```

```

%%%%% FIND COORDINATES OF THE PATCHES OF THE SHEET
%%%%% %

[xo,yo]=coord(a,b,Nx,Ny); % Call function coord.m

x11=reshape(xo,1,Nx*Ny);
y11=reshape(yo,1,Nx*Ny);

%%%%% %
%%%%% %

%%%%% %%% FIND COORDINATES OF THE PATCHES IN DCS
%%%%% %

if choice2==1
    nx=Nx;
    ny=Ny;

    [U,V]=coord(2,2,nx,ny);
    U1=reshape(U,1,nx*ny);
    V1=reshape(V,1,nx*ny);

elseif choice2==0
    nx=4      % Nu
    ny=5      % Nv

    [U,V]=coord(2,2,nx,ny);
    U1=reshape(U,1,nx*ny);
    V1=reshape(V,1,nx*ny);
    sintheta=sqrt(U1.^2 +V1.^2);

    II=find(sintheta>1);
    U1(II)=[]; V1(II)=[];

```

```

end

%%%%% This part finds the index of the selected points
%%%%%

for l=1:length(U1)
    f11=u1-U1(l);
    f21=find(abs(f11)-min(abs(f11))==0);

    f12=v1-V1(l);
    f22=find(abs(f12)-min(abs(f12))==0);

    l1=1;
    ff=f22-f21(l1);
    ff1=find(ff==0);
    while ff1==[]
        l1=l1+1;
        ff=f22-f21(l1);
        ff1=find(ff==0);
    end
    index(l)=f21(l1);
end

%%%%%
UU1=u1(index);
VV1=v1(index);

[UU1' U1' VV1' V1'];

```

```

X1=x1(index);Y1=y1(index);
[X1' x11' Y1' y11'];

sintheta=sqrt(U1.^2 +V1.^2);
pphi=atan2(V1,U1);

ccostheta=sqrt(1-sintheta.^2);

if choice1==1      % Bistatic

    sinc1=sin(k/2*Dx*(U(1,:)+ui))./(k/2*Dx*(U(1,:)+ui));
    S1=find(isnan(sinc1));
    sinc1(S1)=ones(size(S1));

    sinc2=sin(k/2*Dy*(V(:,1)+vi))./(k/2*Dy*(V(:,1)+vi));
    S2=find(isnan(sinc2));
    sinc2(S2)=ones(size(S2));

    ssinc=sinc2*sinc1;
    ssinc=reshape(ssinc,1,nx*ny);
    if choice2==0
        ssinc(II)=[];
    end
    C=[];
    for l=1:Nx*Ny
        e=exp(j*k*(X1*(U1(l)+ui)+Y1*(V1(l)+vi)));
        C=[C;e];
    end

if choice3==1 % Sigma_th_th

EE=E(index);

```

```

E1=EE./(Dx*Dy*cos(thir)*ccostheta.*ssinc.*cos(pphi-phiir));
E1=EE./(Dx*Dy*cos(thir)*ccostheta.*ssinc.*cos(phiir));

Z=find(isnan(E1));
E1(Z)=zeros(size(Z));
E1=conj(E1');
%g=C\E1;
g=pinv(C)*E1;
imp=.5*(1./g-377*cos(thir));
impl=reshape(imp,Ny,Nx);

dd=real(imp);

elseif choice3==2 %sigma_phi_phi

EE=E(index);
E1=EE./(Dx*Dy*cos(thir)*ssinc.*cos(pphi-phiir));
Z=find(isnan(E1));
E1(Z)=zeros(size(Z));
E1=conj(E1');
g=C\E1;
%g=pinv(C)*E1;
imp=(1/(2*cos(thir)))*(1./g-377);
impl=reshape(imp,Ny,Nx);

dd=real(imp);

elseif choice3==3

```

```

E1_th=E_th./(Dx*Dy*cos(thir)*ccostheta.*ssinc);
Z1=find(isnan(E1_th));
E1_th(Z1)=zeros(size(Z1));
E1_th=conj(E1_th');

E1_phi=E_phi./(-Dx*Dy*cos(thir).*ssinc);
Z2=find(isnan(E1_phi));
E1_phi(Z2)=zeros(size(Z2));
E1_phi=conj(E1_phi');
E1=[E1_th;E1_phi];

a11=conj(Eth_i*cos(pphi-phiir))';
a12=conj(Ephi_i*sin(pphi-phiir))';
a21=conj(Eth_i*sin(pphi-phiir))';
a22=conj(-Ephi_i*cos(pphi-phiir))';

Y1=((a12.*E1_phi)-(a22.*E1_th))./((a12.*a21-a11.*a22));
%Y2=(E1_th-a11.*Y1)./a12;

g1=pinv(C)*Y1;
%g2=pinv(C)*Y2;

imp=.5*(1./g1-377*cos(thir));
%imp=1/(2*cos(thir))*(1./g2-377);

impl=reshape(imp,Ny,Nx);
dd=real(imp);

end
save faros dd Dx Dy k x11 choice1 choice3 thir phiir ui

%%%%%%%%%%%%% MONOSTATIC %%%%%%

```

```

elseif choice1==0    % Monostatic

sinc1=sin(k*Dx*U(1,:))./(k*Dx*U(1,:));
S1=find(isnan(sinc1));
sinc1(S1)=ones(size(S1));

sinc2=sin(k*Dy*V(:,1))./(k*Dy*V(:,1));
S2=find(isnan(sinc2));
sinc2(S2)=ones(size(S2));

ssinc=sinc2*sinc1;
ssinc=reshape(ssinc,1,nx*ny);

C=[];
for l=1:Nx*Ny
    e=exp(2*j*k*(X1*U1(l)+Y1*V1(l)));
    C=[C;e];
end

EE=E(index);
E1=EE./(Dx*Dy*ssinc);
Z=find(isnan(E1));
E1(Z)=zeros(size(Z));
E1=conj(E1');
g=C\E1;
%g=pinv(C)*E1;
imp=.5*(1./g-377);
imp1=reshape(imp,Ny,Nx);

dd=real(imp);

save faros dd Dx Dy k x11 choice1 % Use in synth1d.m

```

```
time=toc

end

figure
mesh(XX,YY,real(imp1))
hold on
mesh(xx,yy,r)
hold off
xlabel('x (wavelengths)')
ylabel('y (wavelengths)')
zlabel('Rs and Ros in Ohms')
rerror=max(max(abs(imp1)-r))/max(max(r))
```

%

Code synth1d.m

% This code reads the surface resistivity from the file  
faros.dat

% created by field.m and plots the scattered RCS in the  
principal

% plane phi=0 (u axis).

clear

load faros

sinth=0:(1/49):1; % Sampling the sin (or the dcs)

costh=sqrt(1-sinth.^2);

if choice1==1 % Bistatic

if choice3==1 % Sigma\_th\_th

d=1./(2\*dd+377\*cos(thir));

for p=1:50

expn=exp(j\*k\*(x11\*(sinth(p)+ui)));

s(p)=(expn\*conj(d));

end

sinc1=sin(k/2\*Dx\*(sinth+ui))./(k/2\*Dx\*(sinth+ui));

S1=find(isnan(sinc1));

sinc1(S1)=ones(size(S1));

RCS=(377\*2\*pi\*Dx\*Dy\*cos(thir)\*costh\*cos(phiir).\*sinc1.\*s).^2  
/pi;

elseif choice3==2 % Sigma\_phi\_phi

```

d=1./(2*dd*cos(thir)+377);
for p=1:50
    expn=exp(j*k*(x11*(sinh(p)+ui)));
    s(p)=(expn*conj(d));
end

sinc1=sin(k/2*Dx*(sinh+ui))./(k/2*Dx*(sinh+ui));
S1=find(isnan(sinc1));
sinc1(S1)=ones(size(S1));

RCS=(377*2*pi*Dx*Dy*cos(thir)*cos(phiir)*sinc1.*s).^2/pi;

elseif choice3==3
    brake

end

elseif choice1==0 % Monostatic

    d=1./(2*dd+377);
    for p=1:50
        expn=exp(2*j*k*(x11*sinh(p)));
        s(p)=(expn*conj(d));
    end

    sinc1=sin(k*Dx*sinh)./(k*Dx*sinh);
    S1=find(isnan(sinc1));
    sinc1(S1)=ones(size(S1));

```

```
RCS=(377*2*pi*Dx*Dy*sinc1.*s).^2/pi;

end

RCS1=fliplr(RCS);
RCS=[RCS1 RCS];

theta=asin(sinth);
theta1=fliplr(theta);
theta2=[-theta1 theta];
theta3=theta2*180/pi;
sintheta1=fliplr(sinth);
sintheta2=[-sintheta1 sinth];

figure(1)
plot(theta3,10*log10(abs(RCS)),'r')
```

```

%
% Code fanalys1.m
% This code calculates the FFT of the field
% of methods (I) and (II)

clear
load nf
% Method (I)
x=length(E);
Y1=fft(E);
MM=[Nx Ny];MMM=min(MM);
f1=MMM/2*(0:x/2-1)/x;

% Method (II)
E2=E;
E2(I)=[];
x2=length(E2);
Y=fft(E2);
f2=MMM/2*(0:x2/2-1)/x2;

figure, subplot(211)
plot(f2,abs(Y(1:x2/2)))
%axis([0 3 0 1500]);
xlabel('Nu or Nv'); ylabel('abs(FFT)')

subplot(212)
plot(f1, (abs(Y1(1:x/2)))); %axis([0 3 0 1500]);
xlabel('Nu or Nv'); ylabel('abs(FFT)')

```

```

%           Code fanalys2.,
% This code calculates the FFT of the field
% in u and v directions

clear
load nf

% Method (I) columns
% $E=(377*2*pi*E).^2/pi;$ 
x=length(E);
Y1=abs(fft(E));
MM=[Nx Ny];MMM=min(MM);
f1=MMM/2*(0:x/2-1)/x;

% Method (II) -rows
E2=reshape(E,Ny,Ny);
E2=conj(E');
E2=reshape(E2,1,Nx*Ny);
Y2=abs(fft(E2));

figure, subplot(211)
plot(f1,Y1(1:x/2))
axis([0 5 0 .8]);
xlabel(' Nv'); ylabel('abs(FFT)')

subplot(212)
plot(f1,Y1(1:x/2));
axis([0 5 0 .8]);

xlabel('Nu'); ylabel('abs(FFT)')

```

```

function [xo,yo]=coord(a,b,Nx,Ny)
% Given the dimensions (a) in x, (b) in y of a
% rectangle and the number of segments (Nx) in x
% and (Ny) in y, the coordinates of center of
% each patch is returned.
% Point 0 of the coordinate system is at the
% center of the rectangle.

% Date: 1 Nov 1994
% By: Nick Faros

dx=a/Nx;
dy=b/Ny;

if rem(Nx,2)==0 % i.e. Nx is an even number
    for n=1:Nx
        for i=1:Ny
            xo(i,n)=-(Nx/2-(n-1)-0.5)*dx;
        end
    end
else % if Nx is an odd number
    for n=1:Nx
        for i=1:Ny
            xo(i,n)=-( (Nx-1)/2-(n-1)-0.5)*dx-dx/2;
        end
    end
end

if rem(Ny,2)==0 % i.e. Ny is an even number

    for n=1:Nx
        for i=1:Ny
            yo(i,n)= (Ny/2-(i-1)-0.5)*dy;
        end
    end

```

```
    end
else % if Nx is an odd number

    for n=1:Nx
        for i=1:Ny
            yo(i,n)= ((Ny+1)/2-(i-1)-0.5)*dy-dy/2;
        end
    end
end
```

```

%
%           Code fit.m
%
% This program fits M points in the unit circle.
%
% The spacing is uniform in one or both directions.

%
% Date: 1 Nov 1994
%
% By: Nick Faros.
clear
M=input('Enter number of points in the unit circle: ');

nx=2; ny=2;      % Start at those values.

dx=2/nx;
dy=2/ny;

%
% Find the coordinates of the center
% of the patches.

[u1,v1]=coord(2,2,nx,ny);
u1=reshape(u1,1,nx*ny);
v1=reshape(v1,1,nx*ny);
sintheta=sqrt(u1.^2 +v1.^2);
I=find(sintheta>1);
v1(I)=[];u1(I)=[];
L=length(v1);

k=1;

while L<M
if rem(k,2)==0
    nx=nx+1;
    [u1,v1]=coord(2,2,nx,ny);
    u1=reshape(u1,1,nx*ny);
    v1=reshape(v1,1,nx*ny);
    sintheta=sqrt(u1.^2 +v1.^2);

```

```

I=find(sintheta>1);
v1(I)=[];u1(I)=[];
L=length(v1);

elseif rem(k,2) ~=0
    ny=ny+1;
    [u1,v1]=coord(2,2,nx,ny);
    u1=reshape(u1,1,nx*ny);
    v1=reshape(v1,1,nx*ny);
    sintheta=sqrt(u1.^2 +v1.^2);
    I=find(sintheta>1);
    v1(I)=[];u1(I)=[];
    L=length(v1);
end
k=k+1;
end
[nx ny L]
plot(u1,v1,'*'), xlabel('u'), ylabel('v')
title('Points inside the unit circle')

```

#### LIST OF REFERENCES

1. Senior, T. B. A., "Combined Resistive and Conductive Sheets, " *IEEE Trans. Antennas and Propagation*, Vol. AP-33, no 5, pp. 577-579, May 1985.
2. Jenn, D. C., "Solution of Inverse Scattering Problems Using a Method of Moments Approach, " *Eight Annual Review of Progress in Applied Computational Electromagnetics*, pp. 90, Monterey CA, March 1992.
3. Senior, T. B. A., "Impedance Boundary Conditions For Imperfectly Conducting Surfaces, " *Applied Sci. Res.*, sec B, vol 8, pp. 414, 1960.
4. Bateman, H., *Electrical and Optical Wave Motion*, Cambridge University Press, Cambridge, England, 1915.
5. Balanis, C. A., *Advanced Engineering Electromagnetics*, John Wiley & Sons, Newark, NJ, 1989.
6. Oppenheim A. V., Willsky, A. S. and Young, I. T., *Signals and Systems*, Prentice-Hall, Atlanta, GA, 1983.



## INITIAL DISTRIBUTION LIST

	No. Copies
1. Defense Technical Information Center Cameron Station Alexandria, Virginia 22304-6145	2
2. Library, Code 52 Naval Postgraduate School Monterey, California 93943-5101	2
3. Chairman, Code EC Department of Electrical and Computer Engineering Naval Postgraduate School Monterey, California 93943-5121	1
4. Prof. Michael Morgan, Code EC/Mw Department of Electrical and Computer Engineering Naval Postgraduate School Monterey, California 93943-5121	1
5. Prof. David C. Jenn, Code EC/Jn Department of Electrical and Computer Engineering Naval Postgraduate School Monterey, California 93943-5121	1
6. Prof. Ramakrishna Janaswamy, Code EC/Js Department of Electrical and Computer Engineering Naval Postgraduate School Monterey, California 93943-5121	1
7. Embassy of Greece Naval Attaché 2228 Massachusetts Ave., NW Washington, DC 20008	1
8. Nikolaos I. Faros Thessalonikis 69 St. 18546, Piraeus Greece	2